Androgens contribute to sex bias of autoimmunity in mice by T cell-intrinsic regulation of Ptpn22 phosphatase expression

Jean Lee[1,2], Leonid A. Yurkovetskiy[2,3,9], Derek Reiman[4], Lara Frommer[5], Zoe Strong[2], Anthony Chang[2], George J. Kahaly[5], Aly A. Khan[2,4,6,8] ✉ & Alexander V. Chervonsky[2,3,7] ✉

Autoimmune diseases such as systemic lupus erythematosus (SLE) display a strong female bias. Although sex hormones have been associated with protecting males from autoimmunity, the molecular mechanisms are incompletely understood. Here we report that androgen receptor (AR) expressed in T cells regulates genes involved in T cell activation directly, or indirectly via controlling other transcription factors. T cell-specific deletion of AR in mice leads to T cell activation and enhanced autoimmunity in male mice. Mechanistically, Ptpn22, a phosphatase and negative regulator of T cell receptor signaling, is downregulated in AR-deficient T cells. Moreover, a conserved androgen-response element is found in the regulatory region of *Ptpn22* gene, and the mutation of this transcription element in non-obese diabetic mice increases the incidence of spontaneous and inducible diabetes in male mice. Lastly, Ptpn22 deficiency increases the disease severity of male mice in a mouse model of SLE. Our results thus implicate AR-regulated genes such as *PTPN22* as potential therapeutic targets for autoimmune diseases.

Sexual dimorphism in immunity plays a critical role in mammalian evolution. The immune system in females must be strong to protect the mother from infections during gestation and feeding of the progeny. Females respond better to infections[1–5] and vaccinations[6–8]. The trade-off, however, comes in the prevalence of adverse reactions to vaccination[9,10] and autoimmunity[11–14].

Autoimmune diseases such as systemic lupus erythematosus (SLE) have pronounced sex bias[15,16]. In human type 1 diabetes (T1D)

where overall incidence seems to be similar between sexes[17–19] or even prevalent in males[20], in a particular group of patients with poly-glandular autoimmunity (PGA) exhibits an obvious female bias of T1D[21]. Animal models recapitulate these clinical observations. Several mouse models of SLE also exhibit clear sex bias, with the overall incidence and more severe pathology in females over males[22,23]. In NOD/ShiLtJ (NOD) mouse model of spontaneous T1D, sex bias is evident with an average of 75% incidence of T1D in females, in contrast to an

[1]Committee on Cancer Biology, The University of Chicago, Chicago, IL 60637, USA. [2]Department of Pathology, The University of Chicago, Chicago, IL 60637, USA. [3]Committee on Microbiology, The University of Chicago, Chicago, IL 60637, USA. [4]Toyota Technological Institute at Chicago, Chicago, IL 60637, USA. [5]Department of Medicine I, Johannes Gutenberg University (JGU) Medical Center, Mainz 55101, Germany. [6]Department of Family Medicine, The University of Chicago, Chicago, IL 60637, USA. [7]Committee on Immunology, The University of Chicago, Chicago, IL 60637, USA. [8]Program in Molecular Medicine, University of Massachusetts Chan Medical School, Worcester, MA 01655, USA. [9]Present address: Program in Molecular Medicine, University of Massachusetts Chan Medical School, Worcester, MA 01655, USA. ✉e-mail: aakhan@uchicago.edu; achervon@bsd.uchicago.edu

average of 25% incidence in males by 30 weeks of age in most animals facilities[24]. NOD mice also develop sialitis and thyroiditis, thus, serving as a model for human PGA.

Several factors contribute to the sexual dimorphism of autoimmunity: an incomplete inactivation of X chromosome that increases levels of expression of select genes involved in immunity, and sex hormones, pleiotropic factors controlling the development and function of many organs[12,25–28]. Males' sex hormones (androgens) play a significant role in protection from autoimmunity. In the (NZBxNZW)F$_1$ mouse model of SLE, castration nullified male protection from SLE, whereas supplementation of androgens re-established male protection[29]. Castration of NOD male mice is sufficient to reverse protection from T1D, whereas injections of 5α-dihydrotestosterone (DHT) (an active metabolite of the principal androgen testosterone) can restore protection in castrated males[30]. In in vitro experiments, androgens can directly or indirectly affect various immune cell types including monocytes, macrophages, ILC2 progenitors, neutrophils, mast cells, and T cells[31–33] making understanding of the precise molecular mechanisms of androgen interaction with immune cells in vivo difficult. In addition, environmental factors, such as commensal microbes, can affect the sex bias in autoimmunity[24,34,35]. In the current study, we focused on the influence of androgens on T cells and its contribution to the sexual dimorphism of autoimmunity. We found that AR enhances the expression of the negative regulator of T cell activation, PTPN22 phosphatase. In a model of SLE, males lacking PTPN22 showed an increased disease severity. In the NOD model of T1D, male animals lacking AR in T cells or animals lacking PTPN22 androgen-sensitive regulatory sequence were more susceptible to the disease.

Results

Androgen receptor expression in T cells

Androgens signal primarily (but not exclusively) through the broadly distributed intracellular cognate nuclear hormone receptor, androgen receptor (AR)[36]. To determine whether protective effects of androgens were indeed dependent on AR, we used CRISPR/Cas9 technology to delete AR in NOD mice (Supplementary Fig. 1a). AR-negative males showed T1D incidence similar to that of control females (Fig. 1a). Heterozygosity of females did not make a difference (Fig. 1a). Thus, AR is a principal receptor responsible for protection of males. To identify candidate immune cell types with high AR expression, we used Imm-Gen database[37] and compared the relative expression level of *Ar* gene within the immune cell populations. T cells were the major immune cell population with the highest relative expression of *Ar* (Supplementary Fig. 1b). Among the thymic T cell subpopulations, immature double-negative (DN, CD4$^-$CD8$^-$) and single-positive (SP, CD4$^+$, or CD8$^+$) cells (Figs. 1b, c) displayed the highest level of *Ar* expression. We validated these results by quantitative measurement of *Ar* mRNA expression in DN and CD8SP thymocytes isolated from postpubescent male C57BL/6J (B6J) mice (Fig. 1d) or T1D-prone NOD mice (Supplementary Fig. 1c), and by performing Western blotting analysis of peripheral T and B cells (Fig. 1e, f). Protein expression levels in CD4$^+$ and CD8$^+$ T cells correlated with mRNA expression in SP thymocytes, and AR expression in B cells was not detectable. Moreover, using the NIH epigenetic roadmap project[38], we observed that the chromatin is open and accessible near the *Ar* locus in thymocytes, but closed in B cells, in both humans and mice (Fig. 2a, b).

Thus, the effect of androgens on T cells became the focus of our subsequent analyses.

Functional consequences of AR deletion in T cells

To assess the influence of T cell-specific elimination of AR signaling on autoimmune responses, we generated NOD mice carrying 'floxed' allele of *Ar* using CRISPR/Cas9 approach (Supplementary Fig. 2a). NOD.*Ar* floxed animals were crossed to CD4Cre transgenic NOD mice

to generate a model with T cell-specific deletion of *Ar* (Supplementary Fig. 2b), which was confirmed by Western blotting analysis of peripheral CD8$^+$ T cells (Supplementary Fig. 2c). NOD.*Ar*$^{f/f}$CD4Cre$^+$ females and NOD.*Ar*$^{f/y}$CD4Cre$^+$ males were further crossed to 8.3 TCR transgenic[39] or G9C8 TCR transgenic[40,41] NOD mice. T cells transferred from NOD.*Ar*$^{f/y}$CD4Cre$^+$8.3 mice proliferated stronger than 8.3 T cells from AR-sufficient controls in the PLN of male NOD recipients (Fig. 3a). Similarly, T cells from NOD.*Ar*$^{f/y}$CD4Cre$^+$8.3 and NOD.*Ar*$^{f/y}$CD4Cre$^+$G9C8 male mice proliferated stronger than their AR-sufficient counterparts in response to cognate peptides in vitro (Fig. 3b). That was an important observation indicating that hormone-related phenotype is already imprinted in T cells isolated from the animals and that T cells do not require androgens for the execution of their function. The role of T cell-intrinsic AR signaling was further tested by transfers of polyclonal male T cells with conditional AR KO into male NOD.*scid* mice (Fig. 3c). These cells were more aggressive in transferring T1D compared to Cre$^-$ control T cells. Importantly, we observed CD4Cre$^+$ and Cre$^-$ NOD mice with floxed *Ar* alleles for spontaneous development of T1D (Fig. 3d). Whereas Cre$^+$ female mice did not differ from control females in T1D incidence, Cre$^+$ males had significantly more diabetics compared to control males, although they did not reach the incidence in female mice.

Overall, it became clear that T cell-intrinsic signaling through AR contributes in a measurable way to T1D pathogenesis.

To investigate the consequences of the loss of AR signaling for T cell functional populations, we performed single cell RNA sequencing (SCS) analyses using pancreatic lymph node (PLN) cells from three 8-week-old Cre$^+$ and three Cre$^-$ NOD.*Ar*$^{f/y}$ male mice (Fig. 4a, b). There were apparent shifts in individual clusters of both CD4$^+$ (Fig. 4a) and CD8$^+$ T cells (Fig. 4b). Among CD4$^+$ T cells, two closely related clusters were reduced in Cre$^+$ mice. These clusters represent naïve T cells as they are characterized by heightened expression of transcription factors *Klf2*, *Lef1*, and *Ccr7* chemokine receptor (Supplementary Fig. 2d). Interestingly, cluster 2 containing *FoxP3*$^+$ Tregs was represented similarly between the two groups. CD8$^+$ T cells showed similar distinctions between Cre$^-$ and Cre$^+$ groups (Fig. 4b and Supplementary Fig. 2e). Cre$^-$ mice had more naïve CD8$^+$ T cells (Clusters 1, 6 and 7) characterized by expression of *Klf2*, *Lef1* and *Ccr7*. The Cre$^+$ animals had expanded clusters 0, 8 and 10. Cluster 0 had a high expression of CD69, pointing at activated phenotype of these cells. Cluster 8 cells express *IL-2rb* and *Cxcr3* chemokine receptor and are likely short-lived effector cells (SLEC). Cluster 10 is a small group of cells lacking markers of naïve CD8$^+$ T cells. To characterize T cells lacking AR further, we performed flow cytometry analysis of pancreatic lymph nodes (PLNs). The proportions of naïve and activated T cells (CD62L^{hi}CD44^{lo} and CD62L^{lo}CD44^{hi}, respectively) were skewed towards more activated phenotype in Cre$^+$ CD4$^+$ and CD8$^+$ T cells (Figs. 4c and 4d). Other activation markers (CD25, CD69) were also increased in CD4$^+$ and CD8$^+$ T cells from Cre$^+$ animals (Fig. 4c, d). However, no difference was seen in the FoxP3$^+$CD4$^+$ Treg population (Fig. 4c). Androgens are known to suppress production of IFNγ[42,43]. More CD8$^+$ T cells in Cre$^+$ mice produced IFNγ or IFNγ and TNFα (Fig. 4d). Finally, increased levels of memory precursors (MPECs) and short-lived effector cells (SLECs) were identified in Cre$^+$ CD8$^+$ T cells (Fig. 4e). Previously, an imbalance between male and female MPECs and SLECs has been noted during infection[44]. Thus, the loss of T cell intrinsic AR signaling promotes T cell activation and affects functional T cell populations.

AR-driven regulatory networks in T cells

To identify the genes that may associate with regulatory networks driven by AR, we subjected DN and CD8SP thymocytes (highest expressors of AR) from prepubescent NOD males to ChIP-seq analysis with two independent AR-specific antibodies following ex vivo stimulation with DHT. This genome-wide analysis using quantitative enrichment of sequence tags by Model-based Analysis of ChIP-Seq

(MACS)[45] revealed over 100 DHT-dependent AR binding sites (q-value < 0.05) (Supplementary Table 1) with high confidence in regulatory regions near target genes – promoter region (5 K upstream of transcription start; 21.7%), 5′UTR (5.4%), and intergenic region (31.9%) (Fig. 5a). That was in line with the role of AR in transcriptional regulation of gene expression. Moreover, the majority of binding sites (>60%) were marked with both H3k4me3 and H3k27ac chromatin marks, indicating that the regulatory regions of targets were already poised for transcriptional regulation (Fig. 5b).

Utilizing the list of significant (q-value < 0.05) DHT-dependent AR target genes (Supplementary Table 1), functional enrichment analysis was performed using STRING database[46]. Two notable types of AR targets were identified (Fig. 5c): transcriptional regulators of other genes [e.g. transcription factor TCF1, which is associated with the formation of beta catenin:TCF transactivating complex, and a known AR target[47,48]] and genes directly targeted by AR. In AR-negative thymocytes, TCF1 protein expression was found to be reduced (Fig. 5d) and in castrated mice, a quantitative RT-PCR analysis of genes
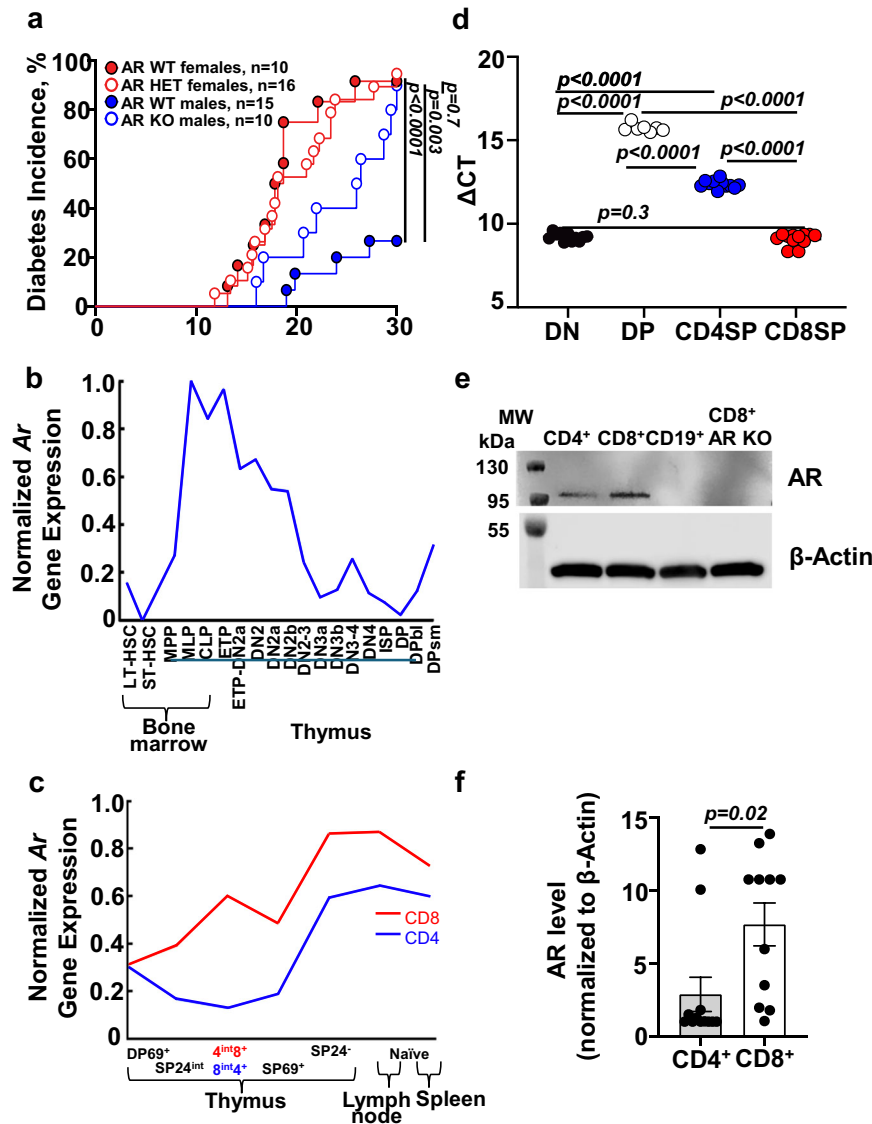
Fig. 1 | Nuclear Androgen Receptor (AR) is responsible for sexual dimorphism of autoimmunity and has variable expression during T cell development.
a Incidence of type 1 diabetes (T1D) in NOD mice: comparison of wild-type females, heterozygous females, wild-type males, and males lacking AR. Significance was calculated using log-rank Mantel-Cox test. n – number of mice. **b, c** Dynamics of *Ar* gene expression during T cell differentiation based on ImmGen data. LT-HSC, Long-Term Hematopoietic Stem Cell; ST-HSC, Short-Term Hematopoietic Stem Cell; MPP, Multi-Potent Progenitor; MLP, Multi-Lymphoid Progenitor; CLP, Common Lymphoid Progenitor; ETP, Early T cell Precursor; ETP-DN2a, Early T cell Precursor – Double Negative 2a; DN2, Double Negative 2; DN2a, Double Negative 2a; DN2b, Double Negative 2b; DN2-3, Double Negative 2-3; DN3a, Double Negative 3a; DN3b, Double Negative 3b; DN3-4, Double Negative 3-4; DN4, Double Negative 4; ISP, Immature Single Positive; DP, Double Positive; DPbl, Double Positive blast; DPsm, Double positive small resting; DP69+, CD69+ Double Positive; SP24int, CD24int Single Positive; 4int8+, CD4intCD8+; 8int4+, CD8intCD4+; SP69+, CD69+ Single Positive; SP24-,

CD24- Single Positive; naïve T cells (CD62LhiCD44-CCR7+). **d** Confirmatory RT-PCR quantification of *Ar* transcript levels in indicated thymic subsets from 8-week-old B6 males. Delta CT (Y-axis) inversely correlates with the strength of expression. Symbols – individual mice. Mean ± sem. *P* values- one-way ANOVA with Tukey's multiple-comparison test. Number of mice: DN n = 11, DP n = 13, CD4SP n = 11, CD8SP n = 7. Combined data from 2 experiments. **e** A representative Western blot image of AR protein levels in CD4+ T cells, CD8+ T cells, CD19+ B cells from peripheral lymph nodes of a 10-week-old NOD male. CD8+ T cells from 10-week-old AR KO male were used as a negative control. β-actin was measured as a loading control. **f** Western blotting quantification of AR protein levels in CD4+ T cells and CD8+ T cells. To combine data from separate experiments, the ratio of optical density of AR band and actin band in wild-type mice was taken as 1.0. Mean ± sem. Significance was calculated using an unpaired *t*-test. Number of mice: CD4+n = 12, CD8+ n = 11. Combined data from 5 experiments.

a   DNaseI hypersensitivity - Mouse

b   DNaseI hypersensitivity - Human
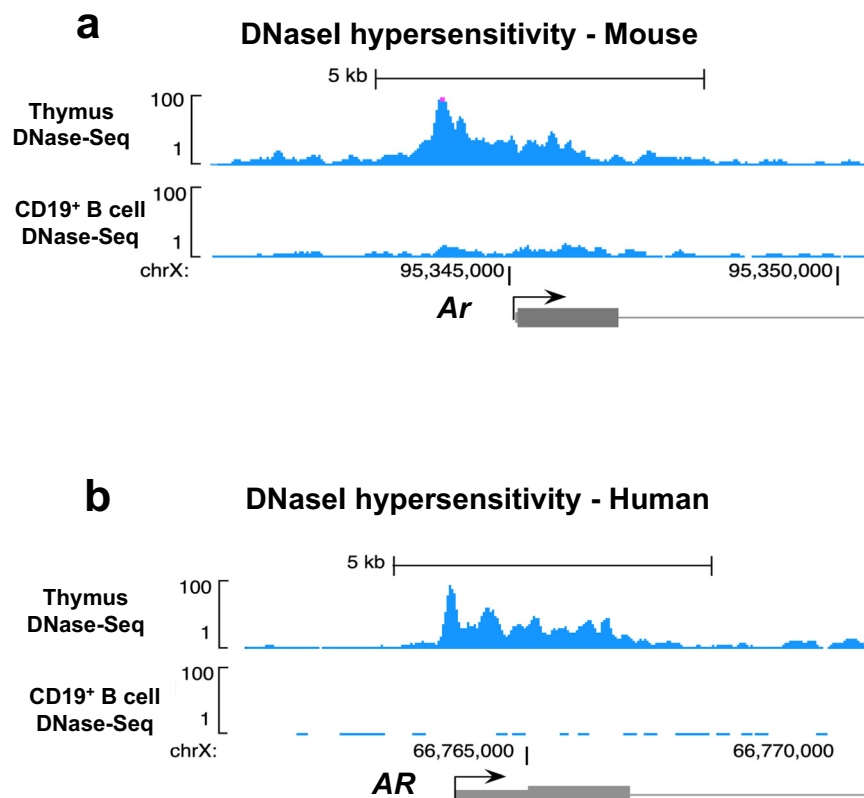
Fig. 2 | DNase I hypersensitive sites around the androgen receptor gene in thymocytes and B cells in mouse and human. Computational analysis of chromatin state at the mouse *Ar* (**a**) and human *AR* (**b**) loci in thymocytes and CD19⁺ B cells. DNase I hypersensitivity was calculated genome-wide in mouse and human. Data obtained from the NIH Roadmap Epigenomics Mapping Consortium. Samples used: human thymus (GSM817172), human CD19⁺ B cells (GSM701507); mouse thymus (GSM1003827), mouse CD19⁺ B cells (GSM1003814).

associated with *Tcf7* (encoding TCF1) showed a reduction of expression of *Axin2* (a prototypic β-catenin regulated gene), of *Ctnnb1* (encoding β-catenin itself) and induction of expression of *Nur77* (a negative regulator of β-catenin) (Fig. 5e, f). A second prominent immunological AR target identified in the center of the STRING network was a TCR signaling-related phosphatase Ptpn22, which is among the top enriched genes in the ChIP-seq analysis (Fig. 5c).

Androgen-AR signaling regulates expression of *Ptpn22* in T cells
In T cells, Ptpn22 regulates proximal TCR signaling events by tuning their strength upon T cell activation[49,50]. In several human genome-wide association studies (GWAS), a coding polymorphism (R620W) in *PTPN22* has been associated with RA, T1D, SLE, and Graves' disease[51–54]. To connect androgen availability with *Ptpn22* expression, we subjected DN and CD8SP thymocytes from castrated or sham-operated B6J mice to qPCR analysis. Expression of *Ptpn22* was consistently higher in mice sufficient in androgens compared to the androgen-deficient counterparts (Fig. 6a). Furthermore, when Jurkat cells (immortalized human T cell line) were transduced with human AR-encoding construct followed by stimulation with an AR agonist R1881, expression of endogenous human *PTPN22* in the presence of the AR agonist was increased (Fig. 6b).

Involvement of Ptpn22 in sexual dimorphism of SLE
We hypothesized that AR-mediated regulation of Ptpn22 leading to modulation of TCR signaling cascade represents a potential mechanism by which androgens reduce autoimmunity in males. To test this hypothesis in a mouse model of systemic sex-biased autoimmunity, we used the B6.NZM mice, a tri-congenic model of SLE generated by the transfer of three lupus susceptibility loci (*Sle1, Sle2,* and *Sle3*) from the

New Zealand Mixed 2410 mice onto the B6 genetic background[55]. B6.NZM mice were crossed to B6.Ptpn22-negative mice[56] and bred to homozygosity for all *Sle* loci (Supplementary Fig. 3a and b). When B6.NZM mice were analyzed for various parameters characteristic of disease progression, sex bias with lower disease penetrance in males was clearly present in agreement with previous reports[23,55] (Fig. 6c). The loss of Ptpn22 correlated best with a loss of the sex bias in the production of anti-nuclear antibodies (ANA). Splenomegaly and overall kidney pathology scores clearly showed a trend for the interaction of Ptpn22 deficiency and sex. At the same time, kidney C3 immune complex deposition was not affected by the Ptpn22 removal in sex-dependent manner (Fig. 6c). The loss of sex bias in Ptpn22-deficient mice was largely due to the increased severity of symptoms in males to a degree similar to that seen in the WT females (Supplementary Fig. 3c). The flow cytometry analysis of T cells and B cells in spleens demonstrated increased CD4⁺ T cell frequencies in the absence of Ptpn22 (Supplementary Fig. 3d). However, the loss of Ptpn22 did not affect the B cell subpopulation frequencies (Supplementary Fig. 3e, f and g). Thus, sexual dimorphism of several (but not all) SLE-associated phenotypes was sensitive to Ptpn22 deficiency.

Identification of a putative *ARE* motif within the upstream regulatory region of *Ptpn22*
To further support the finding that androgen-dependent AR signaling may directly regulate the transcription of *Ptpn22*, we analyzed H3K27ac and H3K4me3 epigenetic marks for open and active chromatin in the AR binding locus of *Ptpn22* identified by ChIP-seq analysis (Fig. 7a). The results suggested positive transcriptional regulation of *Ptpn22* by androgen-dependent AR binding. Thus, we aimed to identify the precise *androgen response element* (*ARE*) motif within the AR
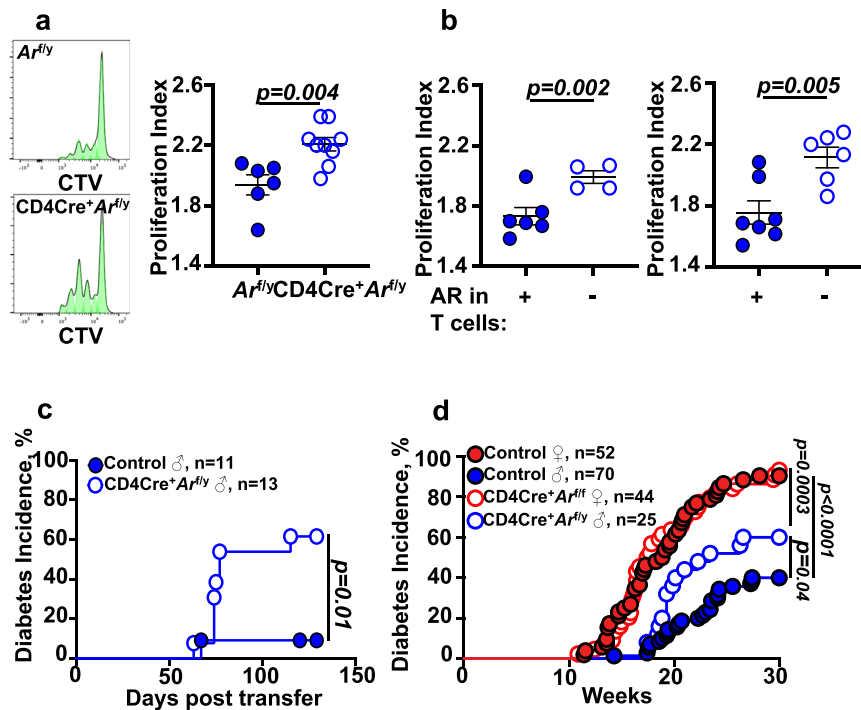
Fig. 3 | T cell-intrinsic AR signaling attenuates T cell autoreactivity. a In vivo proliferation of CTV-labeled CD8⁺ T cells from 8-week-old 8.3.NOD.*Ar^{f/y}*CD4Cre⁻ (filled circles) or Cre⁺ (open circles) male mice in the PLNs of NOD male hosts three days post-transfer. Significance was calculated using an unpaired *t*-test. Symbols – individual mice. Mean ± sem. Combined data from 3 experiments. **b** In vitro proliferation of CTV-labeled CD8⁺ T cells from 8-week-old 8.3.NOD.*Ar^{f/y}* (left) and G9C8.NOD.*Ar^{f/y}* (right) CD4Cre⁺ or Cre⁻ male mice 72 hrs after stimulation with respective peptides. Significance was calculated using an unpaired *t*-test. Symbols – individual mice. Filled circles- Cre⁻ controls, open circles – Cre⁺ mice. Mean ± sem. Combined data from 3 experiments. **c** T1D incidence in male NOD.*scid* recipients of T cells from 8-week-old NOD.*Ar^{f/y}* or NOD.*Ar^{f/y}*CD4Cre⁺ male mice. Significance was calculated using log-rank Mantel-Cox test. **d** Incidence of spontaneous T1D in NOD.*Ar^{f/y}*CD4Cre⁺ or ⁻ littermate males and females. Significance was calculated using log-rank Mantel-Cox test. n – number of mice.

binding site in the upstream regulatory region of *Ptpn22* using a functional luciferase reporter expression assay. Human embryonic kidney 293 T (HEK293T) cells were co-transfected with an *Ar* encoding plasmid and a construct driven by a minimal promoter, in which varying segments of the putative upstream regulatory region of *Ptpn22* were inserted 5′ of luciferase coding sequence. The DNA segment including 1 kb promoter and 5′UTR region of *Ptpn22* induced luciferase expression in response to R1881 treatment, with a 56 bp region near the 3′ end yielding the strongest induction of luciferase expression (Fig. 7b). These results indicated that the 56 bp sequence likely contained a functional *ARE*. This 56 bp sequence was found to be significantly conserved across 60 vertebrate species, implying the presence of a potential critical regulatory function. Accordingly, the corresponding 56 bp region from human *PTPN22* also showed a high induction of promoter activity following stimulation with R1881 (Fig. 7b). The critical sequence was subsequently determined by transfecting human and mouse constructs bearing either truncations or mutations of the 56 bp region. As a result, 5′-GCTNNGCT-3′ sequence in the 5′UTR region was determined to be critical for androgen-AR signaling-dependent *Ptpn22* expression (Fig. 7c).

Regulation of Ptpn22 expression by androgens

To demonstrate that Ptpn22 expression depends on androgens, we used several approaches. First, we castrated male NOD mice and evaluated *Ptpn22* expression by quantitative PCR (Fig. 8a). Its expression was reduced in both DN and SP CD8⁺ thymocytes. Second, we utilized AR-negative mice to measure *Ptpn22* expression in the same subsets of thymocytes (Fig. 8b). The result was the same as in castrated mice: *Ptpn22* expression was downregulated in the absence of AR.
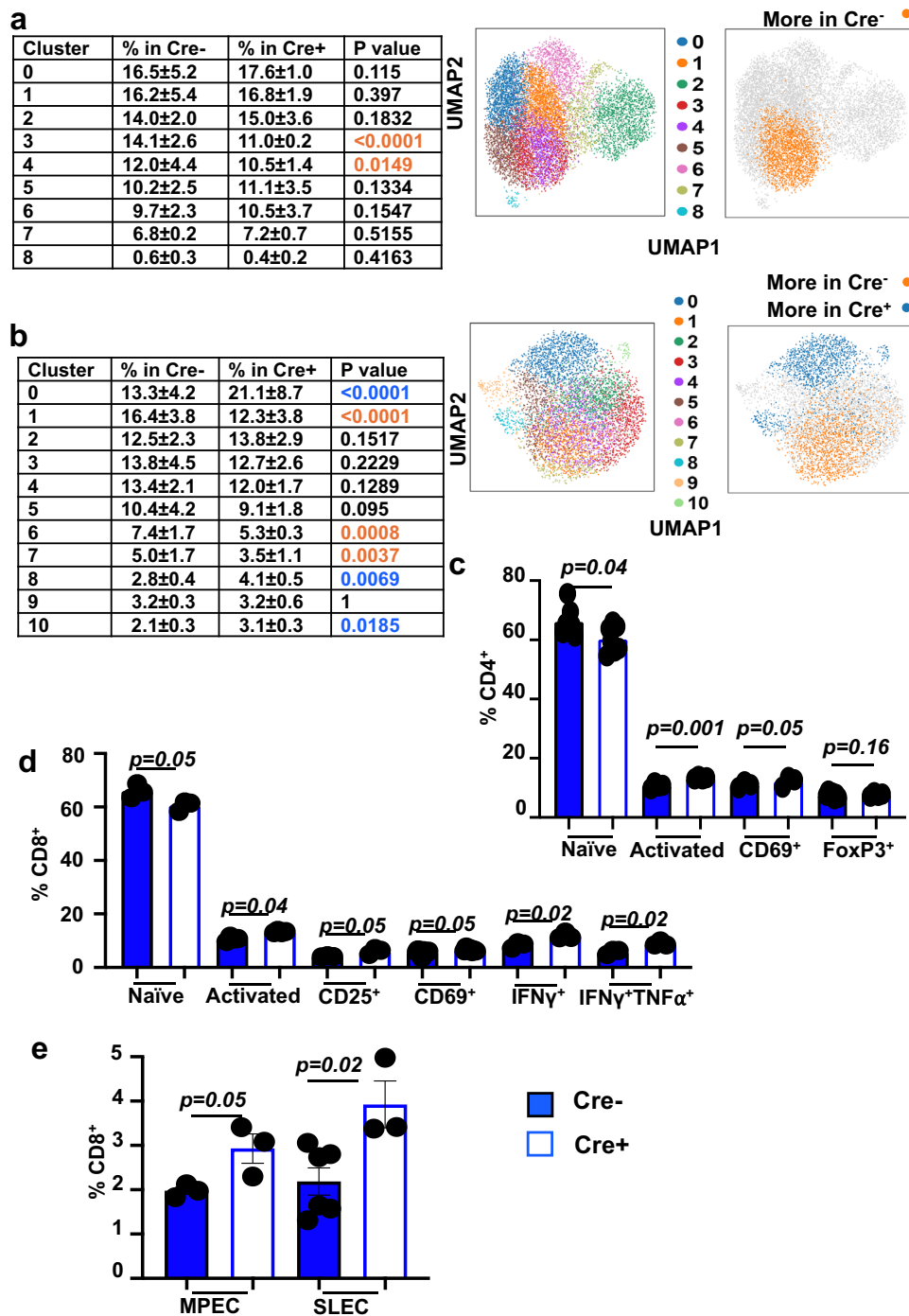
Finally, to test the physiological relevance of the *Ptpn22 ARE* motif identified in vitro, we introduced a mutation into the putative *ARE*

motif of the 5′UTR of *Ptpn22* on the NOD genetic background (NOD.*Ptpn22^{AREmut}*) using the CRISPR/Cas9 approach (Supplementary Fig. 4a). We measured Ptpn22 protein expression in CD8⁺ lymphocytes of WT and mutant males and females by Western blotting. *Ptpn22* KO cells were used as control to ensure antibody specificity. We found PTPN22 expression to be dampened in all females and in mutant males (Fig. 8c). This was also demonstrated at mRNA expression level (Supplementary Fig. 4b).

The disruption of the *ARE* motif altered the antigen-specific proliferative capacity of T cells in vivo. When CTV-labeled insulin-specific T cells from G9C8 TCR transgenic NOD mice of either sex carrying either the wild-type or *Ptpn22^{AREmut}* allele were transferred into intact NOD hosts to track the proliferation of T cells in the PLNs, only male T cells were affected by the disruption of *ARE* and displayed higher capacity to proliferate in response to stimulation by the cognate antigen compared to T cells from wild-type controls (Fig. 9a).

Next, we tested the autoreactive potential of T cells in vivo by transferring them into NOD.*scid* recipients. T cells from NOD.*Ptpn22^{AREmut}* males were highly autoreactive in comparison to T cells from wild-type controls when transferred into male NOD.*scid* recipients, whereas no difference in the overall incidence of T1D was observed between female NOD.*scid* recipients of wild-type (NOD.*Ptpn22^{AREwt}*) and NOD.*Ptpn22^{AREmut}* female T cells (Fig. 9b). These results recapitulate the transfer experiments using AR-negative T cells (Fig. 3c) and provide strong evidence for the in vivo functionality of the identified *ARE* motif in mediating androgen-dependent regulation of T cell autoreactivity by Ptpn22.

To test whether the disruption of *ARE* in the upstream regulatory region of *Ptpn22* alone was sufficient to reverse to any extent the protection from spontaneous T1D in male NOD mice, we observed wild-type and mutant mice for T1D development for 30 weeks.

a

Cluster	% in Cre-	% in Cre+	P value
0	16.5±5.2	17.6±1.0	0.115
1	16.2±5.4	16.8±1.9	0.397
2	14.0±2.0	15.0±3.6	0.1832
3	14.1±2.6	11.0±0.2	<0.0001
4	12.0±4.4	10.5±1.4	0.0149
5	10.2±2.5	11.1±3.5	0.1334
6	9.7±2.3	10.5±3.7	0.1547
7	6.8±0.2	7.2±0.7	0.5155
8	0.6±0.3	0.4±0.2	0.4163

b

Cluster	% in Cre-	% in Cre+	P value
0	13.3±4.2	21.1±8.7	<0.0001
1	16.4±3.8	12.3±3.8	<0.0001
2	12.5±2.3	13.8±2.9	0.1517
3	13.8±4.5	12.7±2.6	0.2229
4	13.4±2.1	12.0±1.7	0.1289
5	10.4±4.2	9.1±1.8	0.095
6	7.4±1.7	5.3±0.3	0.0008
7	5.0±1.7	3.5±1.1	0.0037
8	2.8±0.4	4.1±0.5	0.0069
9	3.2±0.3	3.2±0.6	1
10	2.1±0.3	3.1±0.3	0.0185

Fig. 4 | T cell intrinsic AR signaling shapes T cell functional populations. Unbiased clustering of CD4$^+$ (**a**) and CD8$^+$ T cells (**b**) by Single Cell RNAseq in the PLNs of 8-week-old NOD.$Ar^{f/y}$ or NOD.$Ar^{f/y}$CD4Cre$^+$ male mice. Number of mice: NOD.$Ar^{f/y}$ n = 3, NOD.$Ar^{f/y}$CD4Cre$^+$ n = 3. Clustering was performed aggregating CD4$^+$ or CD8$^+$ T cells from all mice using Leiden clustering. Tables show proportions of cells present in each cluster represented as the mean%± SD across the three replicates in each group, weighted by the number of cells the replicate contributes to the aggregated population of CD4$^+$ or CD8$^+$ T cells for that group. P-values were calculated using a χ^2 test comparing the distribution of cells within and outside each cluster between Cre$^-$ and Cre$^+$ groups. UMAP visualizations depict Ledien clustering as well as clusters enriched in either Cre$^-$ (orange) or Cre$^+$ mice (blue). Top differentially expressed genes characterizing significantly different clusters are shown in Supplementary Fig. 2d, e. **c–e** Flow cytometry analysis of CD4$^+$ (**d**) and CD8$^+$ (**e, f**)

T cells from PLNs of 10-week-old NOD.$Ar^{f/y}$CD4Cre$^-$ (filled bars) and NOD.$Ar^{f/y}$CD4Cre$^+$ (open bars) males. Mean ± sem. Significance was calculated using an unpaired t-test (**c–e**). Single cell PLN suspensions were stained with mAbs specific for CD4, CD8α, CD44, CD62L, CD69, FoxP3, and Fc block and CD8α, CD44, CD62L, CD25, CD69, IFNγ, TNFα, and Fc block, respectively. Naïve, CD4$^+$ or CD8$^+$, CD62L^{hi}CD44^{lo}; activated, CD4$^+$ or CD8$^+$, CD62L^{lo}CD44^{hi}. Number of mice per group, from left to right: (**c**) n = 7, n = 7, n = 4, n = 4, n = 3, n = 3, n = 7, n = 4, and (**d**) n = 3, n = 3, n = 4, n = 4, n = 3, n = 3, n = 10, n = 7, n = 3, n = 3, n = 3. **e** Flow cytometric analysis of CD8$^+$ T cells from PLNs of 10-week-old NOD.$Ar^{f/y}$CD4-Cre$^-$ (filled bars) and NOD.$Ar^{f/y}$CD4Cre$^+$ (open bars) males. Combined data from two experiments. Number of mice: MPEC, NOD.$Ar^{f/y}$CD4-Cre$^-$ n = 3, NOD.$Ar^{f/y}$CD4Cre$^+$ n = 3, SLEC, NOD.$Ar^{f/y}$CD4-Cre$^-$ n = 6, NOD.$Ar^{f/y}$CD4Cre$^+$ n = 3. For gating schemes see Supplementary Fig. 5.
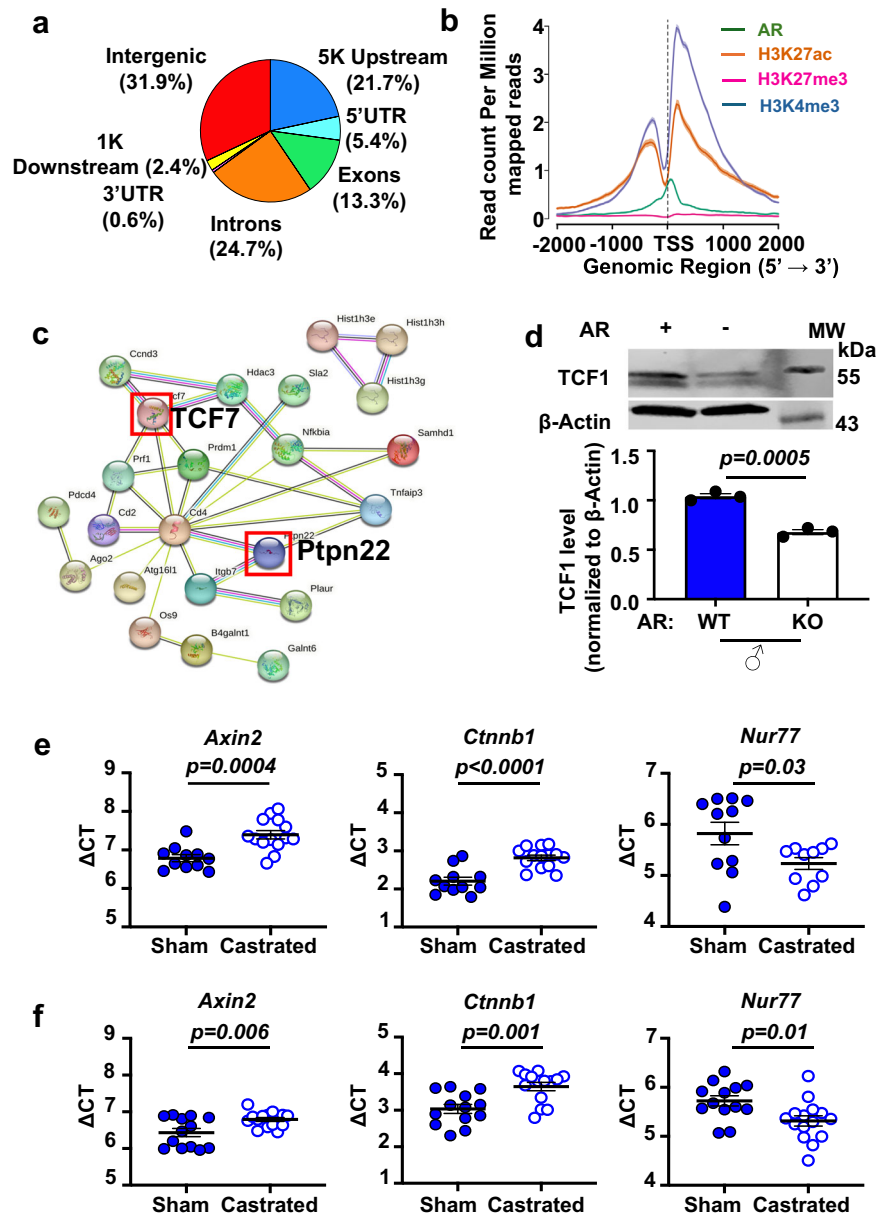
Fig. 5 | Identification of AR target genes in T cells. a Genome-wide distribution of AR binding sites in DN and CD8SP thymocytes identified by ChIP-seq analysis. **b**, Average profile of AR binding and chromatin marks centered at transcription start (TSS) site of AR target genes. **c**, STRING analysis of significant (q-value < 0.05) AR targeted genes. **d** A representative Western blot image (top) of TCF1 protein levels in thymocytes of 10-week-old wild-type and AR-negative males. β-actin was used as a loading control. Summary of Western blot quantification of TCF1 protein levels (bottom) relative to β-actin. Mean ± sem. Significance was calculated using an unpaired *t*-test. Combined data from 3 experiments, n = 3 mice total/group. RT-PCR quantification of genes regulated by β-catenin in DN (**e**) and CD8SP (**f**) thymocytes from 8-week-old B6J males that were either sham-operated or castrated as 4-week-olds. Shown is Delta CT, which is inversely correlated with the strength of expression. Symbols – individual mice. Number of mice: *Axin2*, Sham n = 11, Castrated n = 14, *Ctnnb1*, Sham n = 11, Castrated n = 14, *Nur77*, Sham n = 11, Castrated n = 10 (**e**). Number of mice: *Axin2*, Sham n = 13, Castrated n = 15, *Ctnnb1*, Sham n = 13, Castrated n = 14, *Nur77*, Sham n = 13, Castrated n = 15 (**f**). Combined data from 3 experiments. Mean ± sem. Significance was calculated using an unpaired *t*-test.

NOD.*Ptpn22*[ARE]wt animals developed T1D in a sex-biased fashion (as expected) where females had higher overall incidence than males ($p < 0.0001$, hazard ratio = 7.9). In their littermate mutants, females were prone to diabetes as WT females, but the difference between sexes became less prominent ($p = 0.04$, hazard ratio = 2.6) (Fig. 9c). The result shows significant role of Ptpn22 regulation in the sexual dimorphism of autoimmunity.

To evaluate the influence of Ptpn22 lacking *ARE* on T cell populations, we performed a flow cytometry analyses of T cells in NOD.*Ptpn22*[ARE]wt and NOD.*Ptpn22*[ARE]mut mice. Although no gross differences in the composition of the thymic T cell subpopulations were observed in NOD.*Ptpn22*[ARE]mut males and females (Supplementary Fig. 4c), similar to the profiles of AR-deficient T cells (Figs. 4d, e), the proportions of naïve and activated $CD4^+$ and $CD8^+$ T cells (CD62L^{hi}CD44^{lo} and CD62L^{lo}CD44^{hi}, respectively) in the PLNs were shifted in NOD.*Ptpn22*[ARE]mut males towards more activated phenotype (Fig. 9d). In addition, $CD8^+$ T cell compartment of NOD.*Ptpn22*[ARE]mut males had higher frequencies of $CD25^+$, $CD69^+$, $IFN\gamma^+$, MPEC, and SLEC T cells, a result parallel to the profiles of AR-deficient T cells (Figs. 4e, 4f). We found no significant differences in $CD4^+$ T cells secreting $IL-4^+$ or $IFN\gamma^+$, indicating that the loss of *ARE* by Ptpn22 did not affect T cell polarization in a global fashion (Fig. 9d). However, we cannot exclude
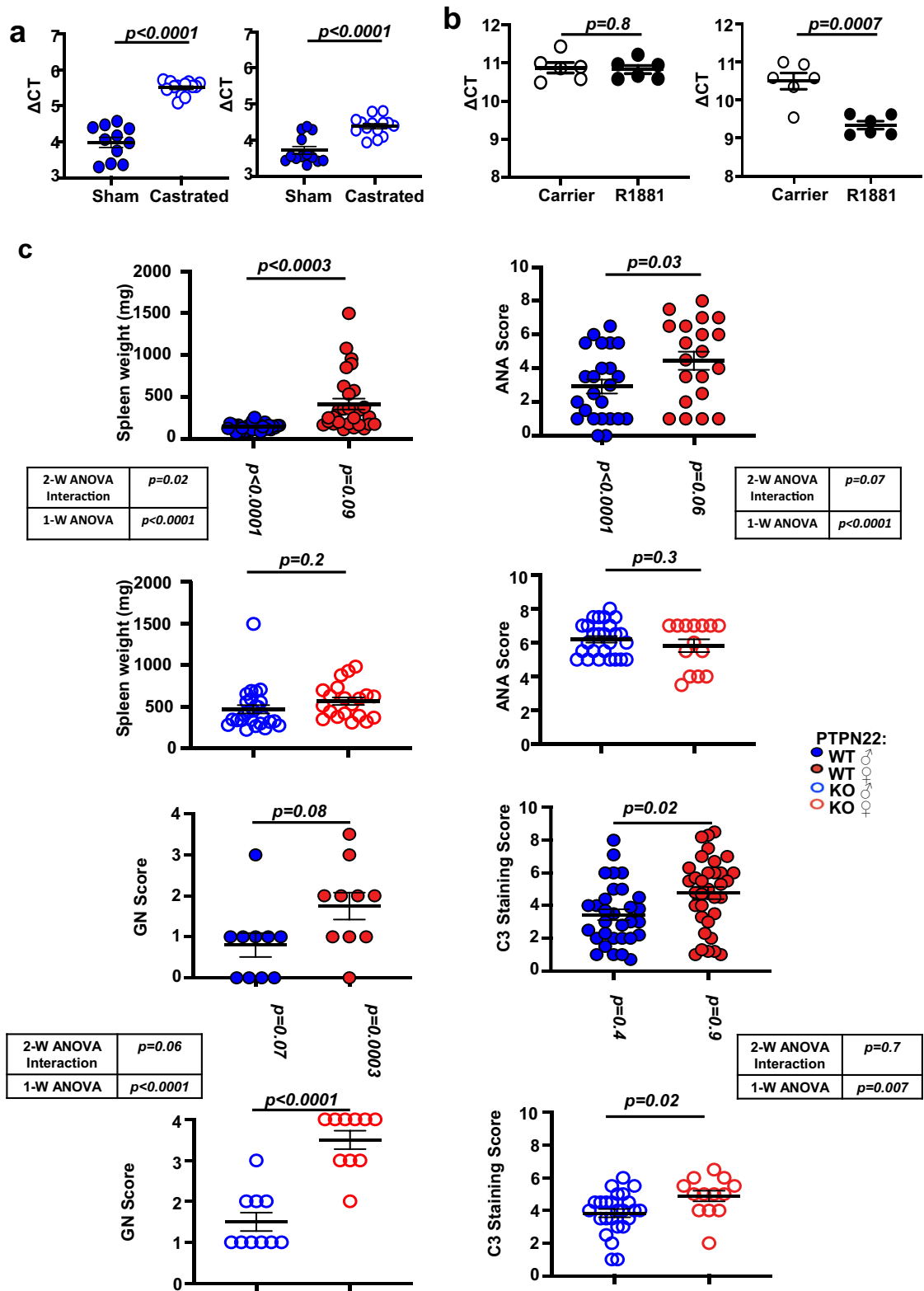
that reactivity to specific triggers (microbial or self) would not be polarized. No difference was observed in FoxP3$^+$CD4$^+$ Treg frequency in the PLNs of NOD.*Ptpn22*^{AREmut} males compared to that of NOD.*Ptpn22*^{AREIwt} males (Fig. 9d), and the 'per cell' suppressive capacity of CD25$^+$CD4$^+$Treg population was not altered (Supplementary Fig 4d). Importantly, changes in T cell functional populations of NOD.*Ptpn22*^{AREmut} was only evident in males but not in females (Supplementary Fig. 4e) emphasizing androgen-mediated regulation of *Ptpn22* via *ARE*.

Regulation of PTPN22 by sex hormones may contribute to the sex bias of autoimmunity in humans

In human population, as mentioned previously, a missense variant (R620W) in PTPN22 has been associated with an increased susceptibility in several autoimmune disorders. The variant changes the properties of PTPN22 protein and does not affect its expression[57]. Thus, we were expecting that this polymorphism will not demonstrate a female sex-biased distribution regardless of the actual bias of the

Fig. 6 | Androgen regulation of *Ptpn22* expression in T cells and the sexual dimorphism in mouse SLE model due to removal of Ptpn22. a RT-PCR quantification of *Ptpn22* transcript levels in DN (left) and CD8SP (right) thymocytes from 8-week-old B6J males that were subjected to sham-operation or castration as 4-week-olds. Mean ± sem. Significance was calculated using an unpaired *t*-test. n – number of mice. Sham n = 11, Castrated n = 14 (left) and n = 13 (right). Combined data from two experiments. **b** RT-PCR quantification of human *PTPN22* transcript levels in Jurkat T cells transduced with either an empty vector (left) or an AR encoding plasmid (right) and treated with R1881 (5 nM) or carrier (0.1% EtOH) for 16 h. Mean ± sem. Significance was calculated using an unpaired *t*-test. Combined data from 2 experiments. n = 6/group. **c** Pathophysiological parameters of SLE measured in 8-10-month-old B6.NZM wild-type (filled circles) and B6.NZM.Ptpn22KO (open circles) male (blue) and female (red) mice: anti-nuclear

antibodies (ANA) scores measured by immunofluorescence of HEp-2 cells with sera diluted 1:100, spleen weights, glomerulonephritis (GN) scores, and complement C3 deposits measured in kidneys using immunofluorescence. *P* values- one-way ANOVA with Tukey's multiple-comparison test between males and females reflecting sex bias are shown horizontally, and values estimating differences between wild-type and KO mice are shown vertically. Number of mice: ANA - WT male n = 24, WT female n = 20, Ptpn22KO male n = 21, Ptpn22KO female n = 16; splenomegaly - WT male n = 44, WT female n = 47, Ptpn22KO male n = 26, Ptpn22KO female n = 23; GN - n =10/group; C3 deposits - WT male n = 49, WT female n = 47, Ptpn22KO male n = 56, Ptpn22KO female n = 29. Mean ± sem. The significance of the interaction between sex and Ptpn22 mutation was calculated using 2-Way ANOVA and the difference in mean values was tested by non-parametric 1-Way ANOVA. Symbols – individual mice.

autoimmune condition. We took two approaches to test this hypothesis. First, we used published summary data on the association for the *PTPN22* R620W variant[58] and the sex bias of the major autoimmune diseases[59] (Fig. 10a, Supplementary Table 2). We observed a striking inverse relationship between sex bias and the reported Odds Ratio (OR) of PTPN22[R620W] allele contribution in major autoimmune diseases. The intrinsic limitation of this analysis is that the two datasets are not matched. To overcome this issue, we analyzed the data from a relatively small, but matched cohort[60–62]. Figure 10b shows the size of the cohort; the ratio between males and females for control and case groups; mutant allele frequencies (heterozygous and homozygous carriers are combined) and χ^2 *p* values for males and females; and the OR for rs2476601. The results showed a lack of sex bias in mutant allele distributions in both sexually dimorphic [Autoimmune Thyroid Diseases, AITD and PGA represented by AITD + T1D] as well as in a non-dimorphic disease (T1D unrelated to PGA).

The overall conclusion from all types of analyses performed here was that *PTPN22* C1858T mutation does not contribute to the female sex bias of the autoimmune diseases emphasizing a possibility that the common allele has the ability to contribute to the sex bias due to hormonal regulation of PTPN22 expression.

Discussion

We previously proposed a model in which both hormonal and environmental signals were required for male protection from autoimmunity and that these signals were not necessarily simultaneous[24]. Thus, hormones may act at early stages of immune cell development. The overview of AR expression in the hematopoietic cells drove our attention to the thymus where AR was previously shown (by antibody staining) to be differentially expressed in thymocytes along their maturation axis[63]. Computational analysis of the AR-binding gene cohort suggested that AR is involved in direct regulation of T cell genes (e.g. *Ptpn22*) or influences entire pathways regulating transcription factors such as *Tcf7*. We focused on the first category. Ptpn22 phosphatase (a.k.a. EST domain-enriched tyrosine phosphatase, or Lymphocyte Phosphatase, LYP, in humans) stood out as a known negative regulator of TCR activation[49,50] and associated with multiple autoimmune disorders[64]. Interestingly, androgens were shown to regulate another regulatory phosphatase Ptpn1[65]. GWAS studies identified a missense variant (rs2476601, R620W) in PTPN22 associated with RA, T1D, and SLE[51–53]. Moreover, genetic manipulation of Ptpn22 resulted in the modulation of autoimmunity in several mouse models[66–68].

AR binding to Ptpn22 regulatory elements suggested that it may play a role in the sexual dimorphism of autoimmunity. In a mouse model of systemic autoimmunity (SLE), B6.NZM mice, some of the manifestations of SLE relevant to T cell functions were found to be sexually dimorphic and Ptpn22-dependent: secretion of ANA and splenomegaly, whereas other manifestations like C3 deposition in the kidney glomeruli were not significantly affected or with a significant increase of severity in females (GN score) showed persistence of sexual dimorphism independent of Ptpn22. These results point at the

contribution of other factors besides Ptpn22 (and likely other cell types) to the overall pathology. Other parameters, such as proportion of marginal zone and follicular B cells were not affected by Ptpn22 deficiency. Although Ptpn22 has been implicated in regulating BCR signaling and B cell tolerance[69–71], these effects may be not AR-dependent due to lack of expression (Fig. 1e) and the inactive state of *Ar* locus in B cells (Fig. 2a, b), or could be secondary to perturbations to T cell signaling caused by Ptpn22 deficiency[56,72]. Thus, even if Ptpn22 signaling has a B cell-intrinsic role, it is unlikely to be sensitive to regulation by sex hormones.

Ptpn22 regulation by sex hormones became a rather attractive hypothesis and led to the search for an AR binding site in *Ptpn22* regulatory elements (Fig. 7). The identified *ARE* sequence (GCTNNGCT) was different from the consensus *ARE* sequence identified by studies of prostate cancer in humans[73,74]. However, *ARE* of multiple genes in multiple tissues have quite variable sequences[75,76]. Localization of *ARE* to the 5'UTR of the gene is also quite common[77,78], including *AR* itself[79]. The short 56 nt sequence containing the GCTNNGCT octamer stimulated higher luciferase expression by itself compared to being a part of a longer sequence (Fig. 7b) pointing at a possible presence of a currently undefined negative regulatory sequence located upstream.

Although the functional significance of the novel *ARE* motif was subsequently validated in vivo, the primary concern was that *ARE* manipulation could affect the overall gene and protein expression regardless of androgen presence. That was not the case, because the lower expression of *Ptpn22* was only detected in mutant male but not female SP thymocytes (Supplementary Fig. 4b) and at the protein level in mature CD8+ T cells (Fig.8c). Although the effect of *ARE* mutation potentially could be observed in multiple cell types where Ptpn22 is normally expressed, T cell intrinsic effect was obvious: T cells from mutant male mice induced T1D efficiently in NOD.*scid* recipient males), whereas transfer of T1D by T cells from mutant females was not different from transfer efficiency of the wild-type female T cells (Fig. 9b).

Ptpn22[AREmut] contributed to the development of the spontaneous disease itself. T1D incidence in NOD.*Ptpn22[AREmut]* females were comparable to that in wild-type females (about 75% at 30 weeks of age). NOD.*Ptpn22[AREmut]* males clearly displayed a trend for increased T1D susceptibility compared to wild-type littermate male controls: the hazard ratios of overall female-to-male incidence were 7.9 in control vs. 2.6 in mutants, respectively, although the cumulative incidence level of T1D in mutant males did not reach that of females (Fig. 9c).

The results are consistent with the hypothesis that AR regulation of *Ptpn22* in males makes T cells less aggressive. Importantly, conditional deletion of AR from T cells led to significant attenuation of T1D in males (Fig. 3d) compared to a pronounced but not statistically significant reduction in NOD.*Ptpn22[AREmut]* male mice ($p = 0.2$), suggesting that AR regulation of Ptpn22 is an important, but not the only, pathway that protects males from autoimmunity. In future experiments, T cell-
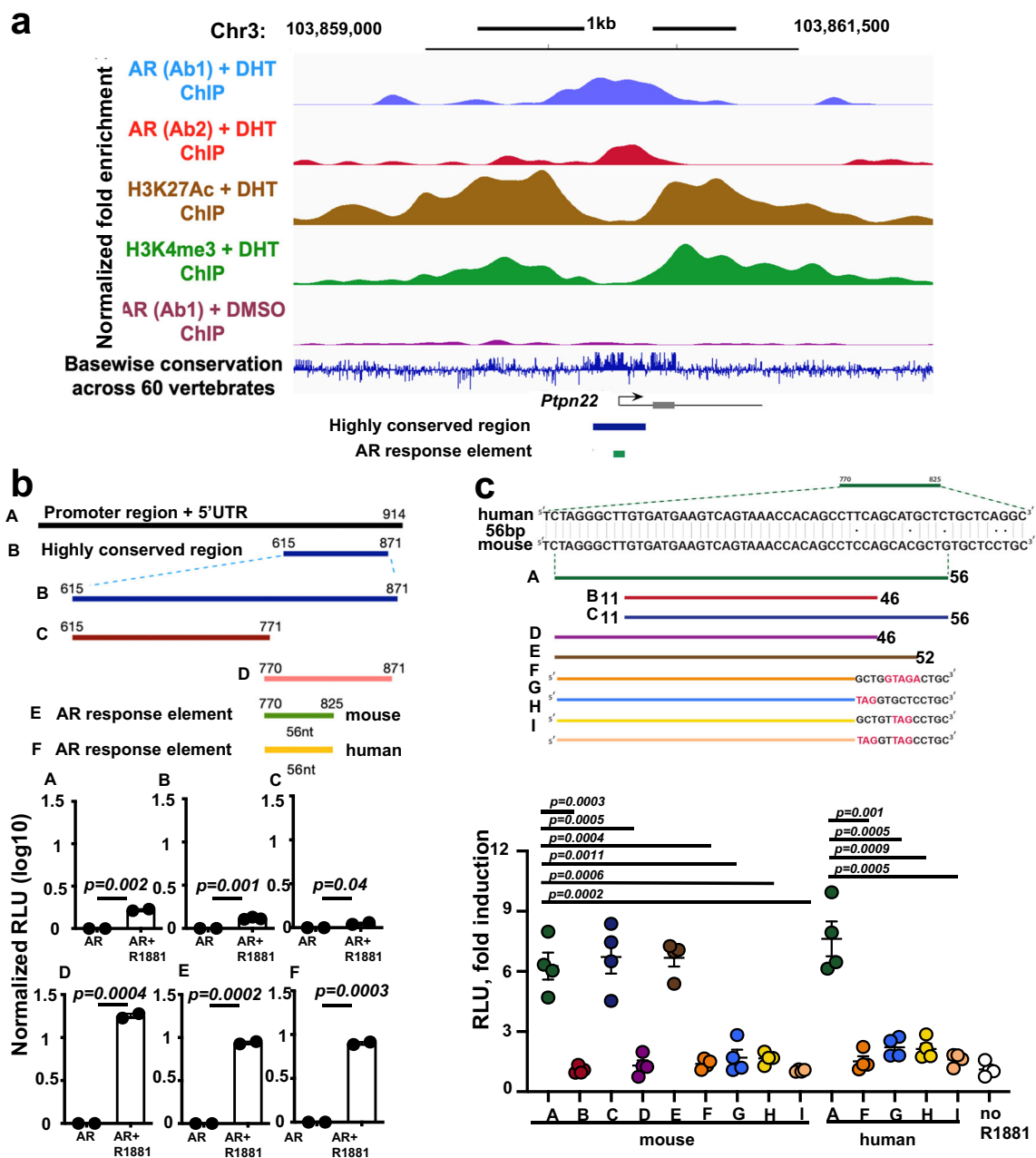
Fig. 7 | Characterization of Androgen Response Element (*ARE*) in the upstream regulatory region of *Ptpn22*. a Normalized fold enrichment of AR based on ChIP-seq experiment in the upstream regulatory region of *Ptpn22* including the state of the chromatin and base-wise conservation across 60 vertebrate species. **b** Schematic diagram of regions tested for AR-mediated *Ptpn22* promoter activity, encompassing 1 kb upstream regulatory site and their respective *Ptpn22* promoter activity measured by luciferase. Mean ± sem. Data from two independent transfection experiments. Significance was calculated using an unpaired *t*-test. ****$p < 0.0001$; ***$p < 0.001$; **$p < 0.01$; *$p < 0.05$. **c** Precise delineation of *ARE* within the conserved 56nt sequence. RLU - relative luciferase units. In all expression tests, HEK293T cells were transiently transfected with mouse or human, wild-type or mutant *Ptpn22* promoter-luciferase reporter plasmid pGL4.23 and pIRES2-zsGreen-1-AR and incubated in the presence or absence of 0.01uM R1881 for 48 h. pRL-CMV was used to control for transfection efficiency. Firefly luciferase levels were normalized to *Renilla* luciferase levels. Mean ± sem. Significance was calculated using an unpaired *t*-test. ****$p < 0.0001$; ***$p < 0.001$; **$p < 0.01$; *$p < 0.05$. Combined data from 4 experiments.

specific KO of AR could be combined with *Ptpn22*^ARE mut and complete Ptpn22 KO to measure precisely the contribution of the hormone-dependent contribution of Ptpn22 in autoimmunity. Other factors involved in the protection of males are likely to synergize and may involve additional T cell-extrinsic mechanisms. It has been shown that transcription factor AIRE expression was sensitive to androgens[80]. AIRE regulates T-cell selection including promotion of Treg differentiation[81] and could be an additional T-cell extrinsic contributor to sexual dimorphism of autoimmunity.

It is important to keep in mind that NOD males are protected from T1D due to the presence of commensal microbiota[24,34]. It would not be realistic to expect that regulation of a single gene like *Ptpn22* by sex hormones would explain the entire sexual dimorphism of the disease, especially given the powerful influence of the microbiota on autoimmunity[24,34,35].

Experiments with in vivo and in vitro cognate peptide-specific proliferation of CD8+ T cells from NOD.*Ar*^f/y CD4Cre+ or Cre− male mice expressing 8.3 or G9C8 TCR transgenes demonstrated stronger
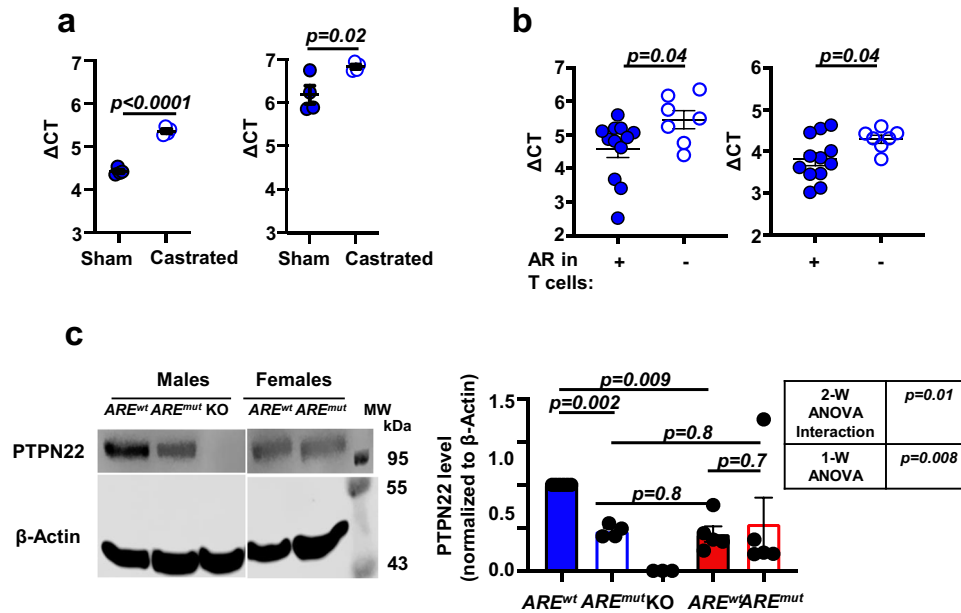
Fig. 8 | Disruption of the *ARE* motif in the 5'UTR of *Ptpn22* modulates its expression in male T cells. male T cell activity and T cell functional populations. a RT-PCR quantification of *Ptpn22* transcript levels in DN (left) and CD8SP (right) thymocytes from 8-week-old NOD males that were either sham-operated (filled circles) or castrated (open circles) as 4-week-olds. Mean ± sem. Significance was calculated using an unpaired *t*-test. Symbols · individual mice. n = 4/group. **b** RT-PCR quantification of *Ptpn22* in DN (left) and CD8SP (right) thymocytes from 8 to 9-week-old NOD AR wild-type (filles circles) and knock-out (open circles) males. Delta CT inversely correlates with the strength of expression. Symbols – individual mice. Combined data from two experiments. Number of mice: AR wild-type n = 12/group, AR KO n = 7/group. Mean ± sem. Significance was calculated using an unpaired *t*-test. The significance of interaction between sex and Ptpn22 mutation was calculated using

2-way ANOVA and the difference in mean values was tested by non-parametric 1-way ANOVA. **c** Left, a representative western blot image (top) of Ptpn22 protein levels in CD8⁺ T cells from peripheral lymph nodes of 10-week-old *Ptpn22^AREwt^* and *Ptpn22^AREmut^* males, females, and CD8⁺ T cells from B6.NZM.Ptpn22KO males were used as a negative control. β-actin was measured as a loading control. Right, a summary of western blot quantification of Ptpn22 protein levels relative to β-actin. Combined data from 4 experiments. Symbols – individual mice. Number of mice: *Ptpn22^AREwt^* male n = 6, *Ptpn22^AREmut^* male n = 4, B6.NZM.Ptpn22KO n = 3, *Ptpn22^AREwt^* female n = 5, *Ptpn22^AREmut^* female n = 5. Mean ± sem. Significance was calculated using 2-way ANOVA and 1-way ANOVA. *P* values- one-way ANOVA with Tukey's multiple-comparison test. Symbols – individual mice. Number of mice: *Ptpn22^AREwt^* male n = 6, *Ptpn22^AREmut^* male n = 4, B6.NZM.Ptpn22KO n = 3, *Ptpn22^AREwt^* female n = 5, *Ptpn22^AREmut^* female n = 5.

proliferation of AR-deficient T cells than AR-sufficient counterparts (Fig. 3a, b). This observation is important, because it argues that androgens make a lasting imprint on T cells in development and the presence of the hormone during activation is no longer required.

In humans, a known R620W mutation in *PTPN22* gene is associated with multiple autoimmune diseases including T1D. It was previously shown[57] that R620 and W620 allelic variants are expressed at a similar level, suggesting a hormone-independent role for the mutant protein. Furthermore, disease risk introduced by that mutation was in *inverse correlation* with the published degree of sexual dimorphism (Fig. 10a). Importantly, the lack of sex bias in mutation distribution is also true for complex autoimmune syndromes in which patients have more than one major autoimmune manifestation (Fig. 10b). In the future, the use of more computationally intensive techniques, such as linkage disequilibrium score regression, could enhance the comparison of phenotypes and aid in determining the heritability of variants. Finally, the same mutation introduced in NOD mice[82] did not affect T1D sex bias. Thus, we posit that this common mutation locks PTPN22 protein in a certain functional state that supersedes the influence of sex hormones. That supports our hypothesis that the most common 'wild-type' allele of PTPN22 could contribute to disease development in a hormone-dependent manner, making this protein and likely multiple other proteins that are controlled by androgens valid targets for therapeutic interventions.

The immune response to modified self in cancer demonstrates similarities with autoimmunity. Several studies have connected AR signaling with exhaustion of anti-tumor CD8⁺ T cell responses limiting the efficiency of immunotherapy[43,47,48]. A negative role of Ptpn22 in anti-tumor immunotherapy has been established in animal models[83,84].

Thus, in addition to autoimmunity, the knowledge of *PTPN22* and other genes' regulation by AR suggests more options for cancer treatment as well.

Methods
Animals
NOD/ShiLtJ (NOD, JAX#001976), NOD.Cg-Tg(Cd4-Cre)1Cwi/2AchJ (NOD.CD4Cre, JAX#013234), NOD.Cg-*Prkdc^scid^*/J (NOD.*scid*, JAX#001303), NOD.Cg-Tg(TcraTcrbNY8.3)1Pesa/DvsJ (NOD.8.3, JAX#005868), C57BL/6J (B6, JAX#000664), B6;NZM-Sle1^NZM2410/Aeg^ Sle2^NZM2410/Aeg^ Sle3^NZM2410/Aeg^/LmoJ (B6.NZM, JAX#007228), and B6.Cg-*Ptpn22^tm2Achn^*/J (B6.Ptpn22⁻/⁻, JAX#028977) mice were purchased from The Jackson Laboratory. NOD.TcraTcrb TgG9C8, NOD.*Ar*KO, NOD.*Ar^f/y^*, and NOD.*Ptpn22^AREmut^* mice produced by us were maintained at the University of Chicago. All animals were kept under SPF conditions at 72-74 °C, 30-70% humidity, and 12 hr/12 hr light cycle. Experimental and control animals were co-housed. Mice were killed by a combination of CO_2 exposure and craniocervical dislocation. These studies have been reviewed and approved by the Animal Care and Use Committee at the University of Chicago.

Human subjects
The subjects used for the association study were described previously[75]. They included 310 white European adult unrelated subjects from four independent cohorts collected from the same region: healthy controls, AITD, T1D, and APS3v (AITD + T1D). Healthy controls tested negative for signs of autoimmune disorders. AITD individuals tested either positive for thyrotropin receptor autoantibodies and hyperthyroidism (Graves' disease) or positive for thyroid peroxidase autoantibodies and hypothyroidism
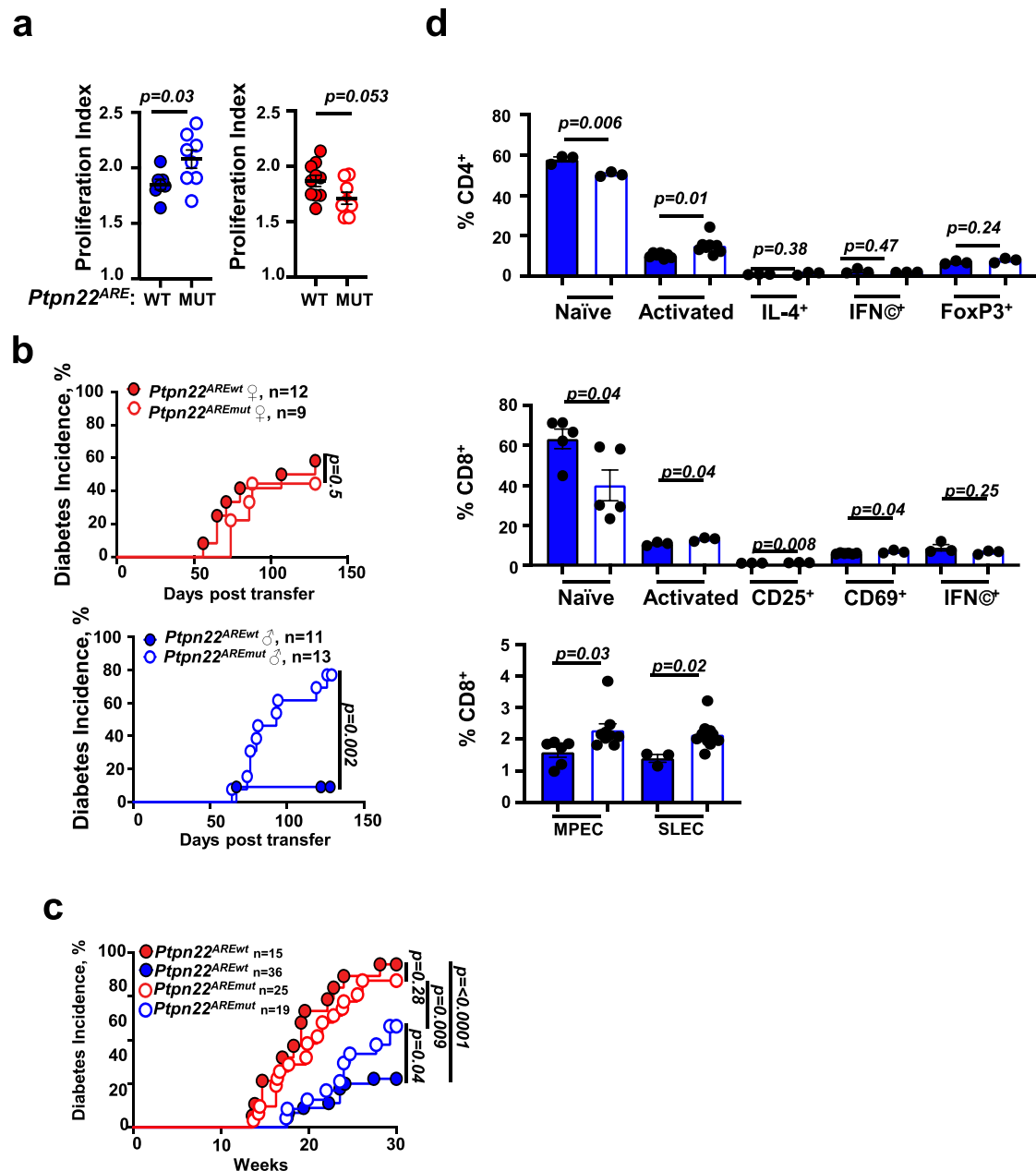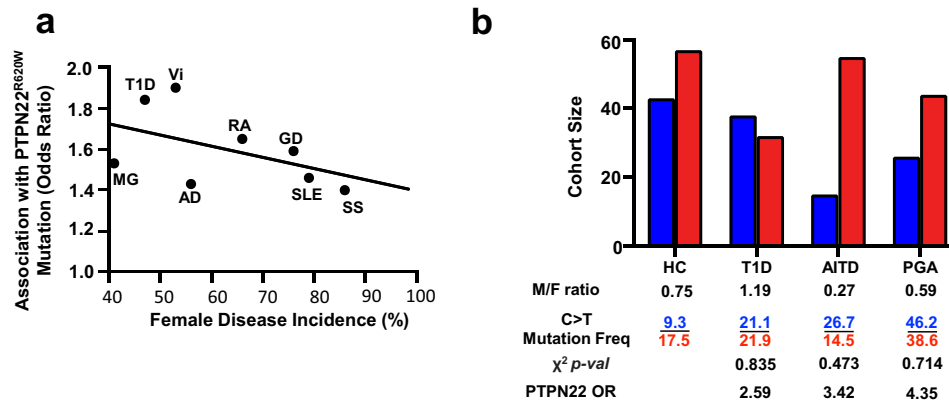
Fig. 9 | Disruption of the *ARE* motif in the 5′UTR of *Ptpn22* modulates male T cell activity and T cell functional populations. a Proliferation of CTV-labeled CD8⁺ T cells from 8-week-old G9C8.NOD.*Ptpn22^AREwt* or G9C8.NOD.*Ptpn22^AREmut* male (blue symbols) and female (red symbols) mice in the PLNs of NOD male and female hosts three days post transfer. Mean ± sem. Significance was calculated using an unpaired *t*-test. The significance of the interaction between sex and Ptpn22 mutation was calculated using 2-Way ANOVA and the difference in mean values was tested by non-parametric 1-way ANOVA. Symbols – individual mice. Number of mice: *Ptpn22^AREwt* males n = 7, *Ptpn22^AREmut* males n = 8, *Ptpn22^AREwt* females n = 10, *Ptpn22^AREmut* females n = 8. Combined data from 3 experiments. **b** T1D incidence in female (left) and male (right) NOD.*scid* recipients of T cells from 8-week-old NOD.*Ptpn22^AREwt* and *Ptpn22^AREmut* female or male mice. Significance was calculated

using log-rank Mantel-Cox test. n – number of mice. **c**, Incidence of spontaneous T1D in NOD.*Ptpn22^AREwt* or NOD.*Ptpn22^AREmut* littermate males and females. Significance was calculated using log-rank Mantel-Cox test. Hazards ratio was calculated using Prism software utilizing Cox proportional hazards regression and was 7.9 for WT female incidence vs. male and 2.6 for *Ptpn22^AREmut* female incidence vs. male. n – number of mice. **d** Flow cytometry analysis of CD4⁺ and CD8⁺ T cells from PLNs of 10-week-old NOD.*Ptpn22^AREwt* or NOD.*Ptpn22^AREmut* male mice. Filled bars - NOD.*Ptpn22^AREwt* males, open bars - NOD.*Ptpn22^AREmut* males. Naïve, CD62L^hiCD44^lo; activated, CD62L^loCD44^hi; MPECs, CD8⁺CD44^intCD62L^hiCD122^hiCD127^hi; SLECs, CD8⁺CD44^intCD62L^intCCR7⁻CD127⁻. Mean ± sem. Significance calculated using an unpaired *t*-test. Combined data from two experiments with a minimum of 3 mice per experiment per group. For gating schemes see Supplementary Fig. 5.

(Hashimoto's thyroiditis) but were negative for pancreatic auto-antibodies. T1D individuals tested positive for complete insulin deficiency and pancreatic autoantibodies but were negative for thyroid autoantibodies. All participants provided informed consent before blood extraction, and the study was approved by the State Ethical Committee of Rhineland-Palatinate.

CRISPR/Cas9-mediated generation of mice

NOD.*Ar*KO, NOD.*Ar^f/y*, and NOD.*Ptpn22^AREmut* mice were produced at the Transgenic and Embryonic Stem Cell Core of the University of Chicago using CRISPR/Cas9 technology. The guides and templates were ordered from Integrated DNA Technologies, Coralville, Iowa. For the homology-directed repair, pUC19 containing the appropriate template

a

b

	HC	T1D	AITD	PGA
M/F ratio	0.75	1.19	0.27	0.59
C>T Mutation Freq	9.3 / 17.5	21.1 / 21.9	26.7 / 14.5	46.2 / 38.6
χ^2 p-val		0.835	0.473	0.714
PTPN22 OR		2.59	3.42	4.35

Fig. 10 | Contribution of the R620W (C1858T) human PTPN22 mutation to autoimmunity is independent of disease' sex bias. a Inverse correlation of the input of PTPN22 mutation associated with autoimmunity (Odds Ratio, OR) and the degree of sexual dimorphism in major human autoimmune diseases (Type 1 diabetes, T1D; Graves' Disease; Vitiligo, Vi; Addison's Disease, AD; Myasthenia Gravis, MG; Rheumatoid Arthritis, AR; Systemic Lupus Erythematosus, SLE; and Sjogren's Syndrome, SS. Based on the compilation of published data[48] and[49]. For the number of human subjects see Supplementary Table 2. **b** Analysis of sexual dimorphism (male/female ratio) in patients with T1D, Autoimmune Thyroid Diseases (AITD), and Polyglandular Autoimmunity (PGA) that manifests as both AITD and T1D in the same patients. Mutation frequencies are shown separately for males (in blue) and females (in red).

was purchased from GenScript Biotech Corporation (Piscataway, NJ) (Supplementary Table 3).

The founder mice were crossed to NOD mice to ensure the germline transmission of the mutant allele and to eliminate possible off-target effects.

Surgical castration
Gonads were excised using Change-A-Tip handheld cauterizer (Bovie Medical Corporation, Clearwater, FL) from 4-week-old males anesthetized with isoflurane. Wounds were closed with Vetbond (3M, Saint Paul, MN). Sham-operated mice had an incision made followed by wound closer with Vetbond (3M).

Diabetes tracking
Diabetes development was monitored by weekly testing of urine glucose with Diastix Reagent Strips (Bayer, Elkhart, IN).

SLE genotyping primers
PCRs specific for the NZM SLE (Sle) 1/2/3 loci mapped to chromosomes 1, 4, and 7 were done with primers at proximal, intermediate, and distal locations of each of these loci. The primers are listed in Supplementary Table 3. PCR results with distal and proximal primers are shown in Supplementary Fig. 3b.

T cell transfer
Single-cell suspensions of lymph nodes and RBC-lysed splenocytes from 8-week-old NOD.*Ptpn22*^*AREwt* or NOD.*Ptpn22*^*AREmut* mice were pooled and subjected to B cell panning, which involved incubation in 10-cm petri dish (Thermo Fisher Scientific, Hampton, NH) pre-coated with 10 µ/ml in-house rabbit anti-mouse IgG antibody for 1 h at RT. Non-adherent fraction was collected and analyzed by FACS to confirm enrichment with T cells. 20×10^6 T cells were i.v. transferred into NOD.*scid* hosts. Diabetes was monitored weekly up to 130 days.

In vitro T suppression assay
CD4^+CD25^+ Treg cells and carboxyfluorescein succinimidyl ester (CFSE, Invitrogen, Carlsbad, CA, cat#C34554)-stained CD4^+CD25^− Tconv cells were cultured together at indicated ratios with irradiated splenocytes and anti-CD3 (Biolegend, cat#100201, clone 17A2) and anti-CD28 (Biolegend, cat#102101, clone 37.51) antibodies (2 µg/ml for each) for 72 hours. Cells were collected and analyzed by FACS for proliferation of CFSE^+CD4^+CD25^− T cells.

T cell proliferation in vitro
2×10^6 cells/ml of RBC-lysed, irradiated splenocytes in 5% FBS (GeminiBio, West Sacramento, CA) supplemented Click's medium (Irvine Scientific, Santa Ana, CA) were seeded in 96-well round bottom tissue culture treated plates (Corning Inc., Corning, NY). Splenocytes were treated with 1 ng/ml LPS (Sigma-Aldrich, Burlington, MA) for 24 h at 5% CO_2 at 37 °C. Splenocytes were washed twice with 5% FBS-supplemented Click's media and 10^5 T cells stained with CellTrace Violet (Invitrogen) using manufacturer's protocol were seeded. 2 µg/ml of cognate peptides (Invitrogen) were added to each well. 72 h later, cells were collected and analyzed by FACS for T cell proliferation.

T cell proliferation in vivo
Single-cell suspensions of lymph nodes and RBC-lysed splenocytes from 8-week-old NOD.*Ptpn22*^*AREwt*G9C8 or NOD.*Ptpn22*^*AREmut*G9C8 mice were pooled and subjected to B cell panning. The resulting T cell fraction was stained with CellTrace Violet (Invitrogen) using manufacturer's protocols. 3×10^6 T cells were i.v. transferred into NOD hosts. After 72 h, PLN and inguinal lymph node (ILN) were isolated from each host and analyzed by FACS for T cell proliferation.

Lymphoid cell isolation, FACS analysis, and sorting
To characterize profiles of T cells and B cells, single cell suspensions prepared from RBC-depleted splenocytes or pancreatic lymph nodes were stained with the following monoclonal antibodies (1:400 unless otherwise noted) using manufacturer's protocols: Fc-Block (BD Biosciences, Franklin Lakes, NJ, cat#553141, clone 2.4G2, Lot#2031746), CD4-FITC (eBioscience, San Diego, CA, cat#11-0041-82, clone GK1.5, Lot#2253007), CD8α-BV421 (Invitrogen, cat#404-0081-82, clone 53-6.7, Lot# 2527379), CD62L-PeCy7 (BioLegend, San Diego, CA, cat#104417, clone MEL-14, Lot# B402916), CD44-APCCy7 (BioLegend, cat#103027, clone IM7, Lot# B308651), CD69-PE (Invitrogen, cat#12-0691-82, clone H1.2F3, Lot# 2009775), CD93-APC (BioLegend, cat#136509, clone AA4.1, Lot# B298565), B220-APCCy7 (BioLegend, cat#103223, clone RA3-6B2, Lot# B308557), IgM-eF450 (Invitrogen, cat#48-5790-82, clone Il/41, Lot# 2172661), CD23-PECy7 (BioLegend, cat#101613, clone B3B4, Lot# B259282), CD21/CD35-FITC (BioLegend, cat#123407, clone 7E9, Lot# B300876), CD1d-PE (Invitrogen, cat#12-0011-82, clone 1B1, Lot# 2129675), and Foxp3-PECy7 (1:200, Invitrogen, 25-5773-82, clone FJK-16s, Lot# 2842549). Dead cells were gated out by staining with propidium iodide (1:2000, Sigma-Aldrich, cat#537060,

Lot# MKCK5162) for surface-stained cells or Zombie Aqua (1:2000, Invitrogen, cat#L34957, Lot# B238036) staining for intracellular stained cells. For intracellular staining, cells were permeabilized after surface marker staining using intracellular fixation and permeabilization buffer set (eBioscience) following the manufacturer's protocol.

To confirm enrichment of T cells from B cell panning, non-adherent fraction was stained with the following monoclonal antibodies (1:400 unless otherwise noted) using manufacturer's protocols: Fc-Block (BD Biosciences, cat#553141, clone 2.4G2, Lot#2031746), CD4-BV421 (eBioscience, cat#404-0042082, clone RM4-5), CD8α-FITC (Invitrogen, cat#MCD0801, clone 5H10, Lot# 2287200), CD19-PE (BioLegend, cat#115507, clone 6D5, Lot# B273503), and B220-APCCy7 (BioLegend, cat#103223, clone RA3-6B2, Lot# B308557) antibodies following the manufacturer's protocol. Dead cells were gated out by staining with propidium iodide (1:2000, Sigma-Aldrich, cat#537060, Lot# MKCK5162).

To measure T cell proliferation, single-cell suspensions of PLN and ILN were stained with the following monoclonal antibodies (1:400 unless otherwise noted) using manufacturer's protocols: Fc-Block (BD Biosciences, cat#553141, clone 2.4G2, Lot#2031746), CD4-FITC (eBioscience, cat#11-0041-82, clone GK1.5, Lot# 2253007), and CD8α-APC (Invitrogen, cat#17-0081-82, clone 53-6.7, Lot# B365419). Dead cells were gated out by staining with propidium iodide (1:2000, Sigma-Aldrich, cat#537060, Lot# MKCK5162). PI⁻CTV⁺CD8α⁺ T cells were gated to calculate the proliferation index.

For sorting thymocyte subpopulations, single cell suspension of the thymus was stained with the following monoclonal antibodies (1:400 unless otherwise noted) using manufacturer's protocols: Fc-Block (BD Biosciences, cat#553141, clone 2.4G2, Lot#2031746), Ter119-Biotin (BioLegend, cat#116203, clone TER-119, Lot# B304958), CD19-Biotin (BioLegend, cat#115503, clone 6D5, Lot# B288401), CD11c-Biotin (Invitrogen, cat#13-0114-82, clone N418, Lot# 2213308), CD11b-Biotin (BioLegend, cat#101203, clone M1/70, Lot# B307868), CD4-FITC (eBioscience, cat#11-0041-82, clone GK1.5, Lot# 2253007), CD8α-BV421 (Invitrogen, cat#404-0081-82, clone 53-6.7, Lot# 2287200), and Streptavidin-APCCy7 (BioLegend, cat#405208, Lot# B258702). Dead cells were discriminated with propidium iodide (1:2000, PI, cat#537060, Lot# MKCK5162) staining. On FACSAria Fusion 5-18 (Becton, Dickinson & Company), PI⁻Ter119⁻CD19⁻CD11c⁻CD11b⁻ cells were sorted into the following populations: DN (CD4⁻CD8⁻), DP (CD4⁺CD8⁺), CD4SP (CD4⁺CD8⁻), and CD8SP (CD4⁻CD8⁺).

For validation of SCS data, single cell suspension of PLN was stained with the following antibodies (1:400 unless otherwise noted) using manufacturer's protocols: Fc-Block (BD Biosciences, cat#553141, clone 2.4G2, Lot#2031746), CD8α-FITC (Invitrogen, cat#11-0081-82, clone 53-6.7, Lot# 2287200), CD44-BV510 (Biolegend, cat#103043, clone IM7, Lot# B298812), CCR7-PE (1:100, Biolegend, cat#120105, clone 4B12, Lot# B387617), CD62L-PeCy7 (Biolegend, cat#104417, clone MEL-14, Lot# B402916), CD127-BV421 (1:100, Biolegend, cat#135023, clone A7R34, Lot# B357148), CD122-PeDazzle (1:100, Biolegend, cat#123217, clone TM-β1, Lot# B396157), CD4-BV421 (Biolegend, cat#100543, clone RM4-5), CD69-FITC (Biolegend, cat#11-0691-82, clone H1.2F3, Lot# B205098), CD25-Biotin (Biolegend, cat#102003, clone PC61, Lot# B229183), Streptavidin-APC (Biolegend, cat#405207, Lot# B384222), IFN-γ-Biotin (Pharmingen, clone XMG1.2, Lot# M072758), Streptavidin-PerCPCy5.5 (Invitrogen, cat#45-4317-80, Lot# B271417), TNFα-BV421 (Biolegend, cat#506327, clone MP6-XT22, Lot# B333754s), IL-4-APC (1:200, Biolegend, cat#504105, clone 11B11, Lot# B384222), and FoxP3-PeCy7 (1:200, Invitrogen, cat#25-5773-82, clone FJK-16s, Lot# 2842549). Dead cells were discriminated with propidium iodide (1:1000, PI, cat#537060, Lot# MKCK5162) staining for surface stains or Zombie Aqua (1:2000, Invitrogen, cat#L34957, Lot# B238036) staining for

intracellular stained cells. For intracellular staining, cells were permeabilized after surface marker staining using intracellular fixation and permeabilization buffer set following the manufacturer's protocol. For cytokine staining, cells were stimulated with Phorbol 12-myristate 13-acetat (PMA) (Sigma) and ionomycin (Sigma) for 4 h at 37 °C prior to staining. All data were acquired using LSRFortessa (Becton, Dickinson & Company, Franklin Lakes, NJ) and analysis was performed using FlowJo software (Becton, Dickinson & Company).

Single cell RNA sequencing sample preparation and data analysis

Pancreatic lymph nodes from three mice per group were harvested and single cell suspensions were prepared. Cells were loaded onto a 10x platform with a target recovery of 10^4 cells per sample for construction of single cell RNA sequence (scRNAseq) library as detailed in 10x Genomics manual. Sequencing was performed on scRNAseq libraries using the Illumina NovaseqX platform at the University of Chicago Genomics Core.

Single cell reads were processed with Cellranger version 6.1.2 using the mm10 version 3.0.0 reference genome. Doublets were removed using the Scrublet Python package. Cells expressing fewer than 200 genes or greater than 2500 genes were filtered out. Additionally, cells whose mitochondrial gene counts contributed to more than 5% of their total counts were removed. Genes observed in fewer than 3 cells were filtered out as well. The remaining cells were total sum scaled to 10,000 counts and log-transformed using a pseudocount of 1. Any cell with a mean expression of CD3δ, CD3ε, and CD3γ greater than 1 was identified as a T cell. CD4⁺ cells were identified as any T cell with positive CD4 expression and CD8a expression equal to 0. Likewise, CD8+ cells were identified as any T cell with positive CD8α expression and CD4 expression equal to 0. Foxp3⁺ cells were identified as CD4⁺ cells with positive Foxp3 expression. CD4⁺ and CD8⁺ cells were then separately visualized with UMAPs using the first 30 PCA components and clustered using Leiden clustering. Clusters with significantly different proportions of Cre⁺ to Cre⁻ cells were identified using Chi-Square tests. Differential gene expression analysis was used to compare expression patterns in Leiden clusters significantly enriched in Cre⁺ or Cre⁻ cells compared to clusters that were not significant. Differential analyses were performed using a t-test with overestimated variance. All analyses were performed using the Scanpy package in Python version 3.9.

Western blotting

Single-cell suspension from pooled lymph node fraction was subjected to magnetic activated cell sorting (Miltenyi Biotec, Bergisch Gladbach, North Rhine-Westphalia, Germany) to enrich for CD4⁺, CD8⁺, or CD19⁺ cells following the manufacturer's protocol. Thymi were homogenized using the Polytron homogenizer (Kinematica Inc., Bohemia, NY) following the manufacturer's protocol. Cells were lysed in buffer containing 1X Tris-buffered saline, 1% Triton-X, and protease inhibitor cocktail (Roche, Basel, Switzerland) and prepared in 1x Laemmli SDS-PAGE buffer. Lysates were run on AnyKD polyacrylamide gel (Bio-Rad, Hercules, CA) and transferred to polyvinylidene difluoride membranes. Membranes were blocked using Phosphate-buffered saline with 0.05% Tween 20 detergent buffer containing 5% milk or 5% BSA. Membranes were probed with primary antibodies at 4 °C overnight. Following list of primary antibodies was used: PTPN22 Rabbit mAb (1:1000, cat#14693S, Lot# 1, Cell signaling technology, Danvers, MA), AR Rabbit mAb (1:2000, cat# 5153T, Lot# 7, Abcam, Cambridge, United Kingdom), and TCF1 Rat mAb (1:500, Biolegend, cat#615701). Membranes were rinsed and incubated with horseradish peroxidase-conjugated secondary antibodies (Jackson ImmunoResearch, West Grove, PA). Membranes were developed using a chemiluminescent substrate and a LI-COR Odyssey Imager (LI-COR Biosciences,

Lincoln, NE). Each protein band was normalized to β-actin using LI-COR Odyssey Imager. Wild-type control ratio of specific band's optical density to the density of actin band was taken as 1.0 to allow to compare multiple experiments. Unprocessed scans of blots are shown in the **Source Data file**.

Histology
Kidney pathology was scored using 5-μm, PAS-stained sections with 40-μm intervals and scored as follows by a renal pathologist: 0, no visible change; 1, focal mesangial proliferative changes; 2, diffuse mesangial proliferative disease; 3, diffuse proliferative glomerulonephritis (GN) with focal crescents; and 4, diffuse GN with crescents in >50% of glomeruli[85,86].

Anti-nuclear Ab staining
HEp-2 slides (Bio-Rad Laboratories, Hercules, CA) were incubated with serum samples diluted at 1:100 in FACS buffer (1% FBS, 0.02% NaN3 in 1XPBS), and counterstained with tetramethylrhodamine-labeled donkey anti-mouse IgG (Jackson ImmunoResearch, West Grove, PA, cat#715-025-151, Lot# 59965)) diluted at 1:100 in FACS buffer. After washes in FACS buffer, slides were wetted with 50% glycerol and covered with glass coverslips (IMEB, San Marcos, CA). The imaging and scoring were performed on the Leica DMLB fluorescent microscope.

Cryosectioning and immunohistochemistry
Kidney samples embedded in OCT (Sakura Finetek USA, Torrance, CA) were cut with a cryostat into 8-μm-thick sections, which were transferred to microscope slides. Slides were fixed in 20 °C acetone, dried, and stained with tetramethylrhodamine-coupled anti-mouse IgG (1:200, Jackson ImmunoResearch, cat#715-025-151, Lot# 59965) or anti-mouse FITC-labeled C3a Ab (1:50, MP Biomedicals, Irvine, CA, cat#55500) in FACS buffer. After washes in FACS buffer, slides were wetted with 50% glycerol and covered with coverglass (IMEB). The slides were stored at 4 °C until imaging using a DMLB microscope (Leica Microsystems, Wetzlar, Germany) equipped with a SPOT camera (Diagnostic Instruments, Sterling Heights, MI).

RNA extraction, reverse transcription, and RT-PCR
Total RNA was extracted for RT-PCR analysis from thymocytes and Jurkat cells with Purelink RNA mini kit (Thermo Fisher Scientific) following manufacturer's instructions. RNA was retrotranscribed using Superscript IV reverse transcriptase (Invitrogen) according to the manufacturer's instructions. cDNA was amplified with specific primers for the mouse genes *Ar*, *Ptpn22*, *Axin2*, *B-Cat*, *Nur77*, and *Actin* using TaqMan Probes (Thermo Fisher Scientific, cat#4331182) or iTaq Universal SYBR Green Supermix (Bio-Rad Laboratories) on QuantStudio 3 Real-Time PCR System (Applied Biosystems, Waltham, MA).

Transient transfection
HEK293T cells were seeded into 24-well plates (Corning, Corning, NY) at a density of 3×10^4 cells/well, cultured for 24 h to 70% confluence, and co-transfected with pGL4.23 mouse *Ptpn22* promoter-luciferase reporter plasmid or pGL4.23 human *PTPN22* promoter-luciferase reporter plasmid, pIRES2-zsGreen-1-AR, and pRL-CMV. pRL-CMV was used as an internal control for transfection efficiency. Transfection was performed with Lipofectamine LTX (Thermo Fisher Scientific) according to the manufacturer's instructions. Complexes were incubated for 20 min at RT prior to transfection. Cells were incubated at 37 °C for 24 h before treatment with 10 nM of R1881. At 48 h post transfection, cells were collected for luciferase assay.

Molecular cloning
Mouse *Ptpn22* promoter and AR sequences were amplified from the tail DNA of NOD/ShiLtJ prepared using DirectPCR Lysis Reagent (Viagen Biotech, Los Angeles, CA). Human *PTPN22* 56 bp promoter

sequence was generated by annealing sense and antisense oligonucleotides (Sigma-Aldrich) to be used as an insert in the ligation reaction. *Ptpn22* promoter sequences with KpnI and XhoI sites were cloned into pGL4.23 vector plasmid digested with KpnI and XhoI (New England Biolands, Ipswich, MA). Digested products were gel purified with NucleoSpin Gel and PCR Clean-up kit (Macherey-Nagel, Düren, Germany) according to the manufacturer's protocol. Insert and vector were ligated with T4 DNA ligase (Invitrogen) and introduced into *E. coli* DH5α (Invitrogen) by electroporation. Colonies grown on Luria-Bertani (LB) agar supplemented with ampicillin (Amresco, Dallas, TX) plates was screened by QIAprep Spin Miniprep Kit (Qiagen, Hilden, Germany). *E. coli* carrying the pGL4.23 reporter with insert were grown overnight at 37 °C in LB broth supplemented with ampicillin. Plasmids were isolated with NucleoBond Xtra Midiprep kit (Macherey-Nagel) and sequenced. Cloning and sequencing primers as well as mouse and human ARE sequences are shown in Supplementary Table 3.

Dual-luciferase assay
Luciferase expression was measured using Dual-Luciferase Reporter Assay System (Promega, Madison, WI) according to the manufacturer's protocol. Briefly, HEK293T cells (CRL11268, American Type Culture Collection, ATCC) were washed in 1xPBS and harvested in 65 μl of 1x reporter lysis buffer, lysed for 15 minutes at RT on a shaker. 20 μl of lysates were used for the measurements of firefly and *Renilla* luciferase activities on a SpectraMax M3 luminometer (Molecular Devices, San Jose, CA). The firefly luciferase activities were normalized to *Renilla* luciferase activities.

AR stimulation in Jurkat cells
The androgen receptor was cloned from pLENTI6.3/AR-GC-E2325 (Addgene, Watertown, MA) by PCR into lentiviral expression plasmid pscALPS-Puro (Addgene). For lentivirus production, HEK293 (CRL-1573, ATCC) cells were seeded at 80% confluency in 6 well plates and transfected with 2.5 μg of total plasmid DNA with either pscALPS-Puro (empty plasmid control) or pscALPS-puro expressing AR, psPAX2 *gagpol* expression plasmid, and the pMD2.G VSV-G expression plasmid at a DNA ratio 4:3:1 using TransIT-LT1 lipid reagent (Mirus Bio LLC, Madison, WI) according to manufacturer protocol. Media was changed to FBS-supplemented RPMI 16 h following transfection, and viral supernatant was harvested 2 days later to be filtered through a 0.45μm filter. To generate AR expressing and control cells, 10^6 Jurkat cells (TIB-152, ATCC) were plated in 1 mL of FBS supplemented RPMI to which 500 μL of viral supernatant was added, followed by selection with 1 μg/mL puromycin 2 days later.

Jurkat cells transduced with AR-encoding construct or empty plasmid were grown to 60% confluence in Click's medium supplemented with 5% FBS. Cells were washed twice with serum-free Click's medium and seeded in 6-well plates (Corning) using Click's medium supplemented with 5% charcoal-stripped FBS (Thermo Fisher Scientific) at 1.75×10^5 cells/well. After incubation for 48 h in 37° CO_2 incubator, cells were stimulated with R1881 (Sigma-Aldrich) (5 nM) or carrier (0.1% EtOH) for 16 h in 37° CO_2 incubator. At the end of the incubation period, cells were harvested and lysed for RNA extraction following the manufacturer's protocol.

Chromatin Immunoprecipitation (ChIP)
Chromatin was cross-linked and immunoprecipitated (ChIP-ed) with antibodies against AR using two distinct antibodies recognizing different epitopes of the AR protein. Antibody 1 (Ab1) targeted an epitope corresponding to amino acids 91-370 of AR (#sc-13062, Santa Cruz Biotechnology, Inc., Dallas, TX), while Antibody 2 (Ab2) recognized an epitope mapping to the N-terminus of AR (#sc-816, Santa Cruz Biotechnology, Inc.). ChIP was performed with Ab1 and Ab2 in the presence of 100 nM DHT in DMSO for 4 hours in DHT-treated samples. Additionally, ChIP with Ab1 was conducted in untreated

samples using only DMSO for 4 hours. ChIP for chromatin marks, including H3K27ac (#39133, Active Motif, Carlsbad, CA, Lot #01613007), H3K4me3 (#39915, Active Motif, Carlsbad, CA, Lot #01713005), and H3K27me3 (#39155, Active Motif, Carlsbad, CA, Lot #01613015), was also performed in the presence of 100 nM DHT in DMSO for 4 hours. For each ChIP reaction, approximately 3 × 10^7 cells were fixed, washed, and snap-frozen following the Cell Fixation protocol from Active Motif (http://www.activemotif.com/documents/1848.pdf). ChIP and DNA sequencing (ChIP-seq) for AR were conducted by Active Motif (Carlsbad, CA). Input chromatin from untreated thymi, ChIP for H3K27ac/H3K4me3/H3K27me3 marks, and AR Ab1 from DMSO untreated samples were processed[76] and sequenced at the Institute for Genomics and Systems Biology at the University of Chicago.

ChIP-seq data processing
Sequencing data from ChIP-seq were first aligned to the mm10 genome using BWA (version 0.7.17-r1188). DHT-dependent AR binding peaks were identified by quantitative enrichment of sequence tags using Model-based Analysis of ChIP-Seq (MACS, version 3.0.0a6), with reads from input chromatin as control. Non-specific binding sites were filtered out using Bedtools (v2.30.0), by removing DHT-dependent AR binding sites that overlapped with the mm10 ENCODE blacklist[87], which lists genomic regions known to often produce artifact signals in functional genomics assays. AR binding sites were determined using an intersection of peaks identified by MACS for Ab1 and Ab2 via Bedtools. The genomic location and distance of binding sites from the nearest transcription start site were analyzed using PAVIS[88] and derived from the mm10 genome. These sites were assigned to genes within 5k upstream and 1k downstream of the mm10 annotated transcription start and end sites. Pathway analysis of these genes was performed using the STRING[46] and Reactome[89] databases.

ChIP peaks and basewise genomic conservation across vertebrates were visualized using bamCoverage (version 3.5.1) and the Integrative Genomics Viewer. ChIP-Seq tracks were smoothed using a moving average with a window of 20 base pairs. PhyloP conservation scores from the alignment of 60 different vertebrates were obtained from UCSC and visualized with the ChIP-Seq tracks. DNase I hypersensitivity information for the Ptpn22 locus in human and murine thymus was obtained from ENCODE[38] and visualized using UCSC genome browser.

ImmGen analysis
To determine the relative *Ar* expression level in cells of the hematopoietic lineage, nearly 200 different myeloid and lymphoid immune cell types curated by the ImmGen consortium[37] were downloaded and analyzed. Log gene expression intensity was centered by subtracting the average expression across all cells, and then min-max normalized to an interval between 0 and 1. All calculations were performed using Matlab (version R2020a).

PTPN22 rs2477601 (R620W) association analysis
The published epidemiological data reporting the percentage of female incidence in autoimmune diseases[25] and the published odds-ratios of autoimmune diseases significantly associated with the common C1858T (rs2477601) R620W nonsynonymous single nucleotide polymorphism of PTPN22 in various GWAS studies[58] were linked based on disease name. Linear regression trend lines were generated using the best-fit line utilizing Python's *Seaborn* package.

Genotyping human subjects
Genotyping procedures for the subjects used in the association study were described previously[60]. In brief, DNA from peripheral venous blood was extracted using QIAamp Blood Mini Kit (Qiagen). Exon 14, which has the SNP C1858T (rs2476601), was amplified by PCR. PCR

products were treated with ExoSAP-IT (USB Europe, Staufen, Germany) and sequenced with an ABI PRISM 3100 Genetic Analyzer (Applied Biosystems, Darmstadt, Germany) following the manufacturer's protocol. Data was analyzed using GeneMapper software version 3.2 (Applied Biosystems).

STRING functional enrichment analysis
A list of significant (q-value < 0.05) AR target genes from ChIP-seq analysis was subjected to STRING[46] analysis. Genes were analyzed for enrichment for Functional Set and Pathway.

Statistical analysis
Statistical analyses were performed with Prism 9 (GraphPad) unless mentioned otherwise. Sequencing data from ChIP-seq were first aligned to the mm10 genome using BWA (version 0.7.17-r1188). ChIP peaks and basewise genomic conservation across vertebrates were visualized using bamCoverage (version 3.5.1) and the Integrative Genomics Viewer. Single-cell reads were processed with Cellranger version 6.1.2 using the mm10 version 3.0.0 reference genome and analysed using the Scanpy package in Python version 3.9.

We conducted two-sided tests for all analyses. Results are expressed as means ± SEM. The statistical difference between the two groups was determined by unpaired *t* test. T1D incidence data was analyzed by Kaplan-Meier. A *p* value < 0.05 was considered statistically significant. Hazards ratio was calculated with Prism-9 using Cox proportional hazards regression.

For PTPN22 R620W association study (AITD, T1D, APS3v), all statistical analyses were performed with SPSS software package, release 15.0 (SPSS Inc., Chicago, IL). Genotypes of each cohort were tested for deviation from Hardy-Weinberg equilibrium with chi-square tests.

Significance of interaction between sex and Ptpn22 mutation was calculated using 2-Way ANOVA and the difference in mean values was tested by non-parametric 1-Way ANOVA using Prizm 9 software.

Reporting summary
Further information on research design is available in the Nature Portfolio Reporting Summary linked to this article.

Data availability
ChIP-seq and single-cell RNA-Seq datasets have been deposited to GEO using accession numbers GSE234134 and GSE271153, respectively. Public databases used to extract gene expression and DNase I sensitivity data are referenced. All data produced by this study are provided in Source Data file. Source data are provided with this paper.

References
1. Yuan, L. et al. Gender associates with both susceptibility to infection and pathogenesis of SARS-CoV-2 in Syrian hamster. *Signal Transduct. Target Ther.* **6**, 136 (2021).
2. Poulin, R. Sexual inequalities in Helminth infections: A cost of being a male? *Am. Nat.* **147**, 287–295 (1996).
3. van Lunzen, J. & Altfeld, M. Sex differences in infectious diseases-common but neglected. *J. Infect. Dis.* **209**, S79–S80 (2014).
4. Guerra-Silveira, F. & Abad-Franch, F. Sex bias in infectious disease epidemiology: patterns and processes. *PLoS One* **8**, e62390 (2013).
5. Fish, E. N. The X-files in immunity: sex-based differences predispose immune responses. *Nat. Rev. Immunol.* **8**, 737–744 (2008).
6. Flanagan, K. L., Fink, A. L., Plebanski, M. & Klein, S. L. Sex and gender differences in the outcomes of vaccination over the life course. *Annu Rev. Cell Dev. Biol.* **33**, 577–599 (2017).
7. Fink, A. L. & Klein, S. L. Sex and gender impact immune responses to vaccines among the elderly. *Physiology* **30**, 408–416 (2015).
8. Furman, D. et al. Systems analysis of sex differences reveals an immunosuppressive role for testosterone in the response to influenza vaccination. *Proc. Natl Acad. Sci. USA* **111**, 869–874 (2014).

9. Green, M. S. et al. Gender Differences in adverse events following the Pfizer-BioNTech COVID-19 vaccine. *Vaccines* **10**, 233 (2022).

10. Markle, J. G. & Fish, E. N. SeXX matters in immunity. *Trends Immunol.* **35**, 97–104 (2014).

11. Whitacre, C. C. Sex differences in autoimmune disease. *Nat. Immunol.* **2**, 777–780 (2001).

12. Billi, A. C., Kahlenberg, J. M. & Gudjonsson, J. E. Sex bias in autoimmunity. *Curr. Opin. Rheumatol.* **31**, 53–61 (2019).

13. Yurkovetskiy, L. A., Pickard, J. M. & Chervonsky, A. V. Microbiota and autoimmunity: exploring new avenues. *Cell Host Microbe* **17**, 548–552 (2015).

14. Weckerle, C. E. & Niewold, T. B. The unexplained female predominance of systemic lupus erythematosus: clues from genetic and cytokine studies. *Clin. Rev. Allergy Immunol.* **40**, 42–49 (2011).

15. Tedeschi, S. K., Bermas, B. & Costenbader, K. H. Sexual disparities in the incidence and course of SLE and RA. *Clin. Immunol.* **149**, 211–218 (2013).

16. Krasselt, M. & Baerwald, C. Sex, symptom severity, and quality of life in rheumatology. *Clin. Rev. Allergy Immunol.* **56**, 346–361 (2019).

17. Sarfo-Kantanka, O. et al. Trends in type 1 diabetes diagnosis in Ghana. *Int Health* **14**, 442–446 (2022).

18. Diaz-Valencia, P. A., Bougneres, P. & Valleron, A. J. Global epidemiology of type 1 diabetes in young adults and adults: a systematic review. *BMC Public Health* **15**, 255 (2015).

19. Zabeen, B. et al. Incidence of diabetes in children and adolescents in Dhaka, Bangladesh. *J. Pediatr. Endocrinol. Metab.* **34**, 509–515 (2021).

20. Ostman, J. et al. Gender differences and temporal variation in the incidence of type 1 diabetes: results of 8012 cases in the nationwide Diabetes Incidence Study in Sweden 1983-2002. *J. Intern Med* **263**, 386–394 (2008).

21. Hansen, M. P., Matheis, N. & Kahaly, G. J. Type 1 diabetes and polyglandular autoimmune syndrome: A review. *World J. Diab.* **6**, 67–79 (2015).

22. Peeva, E., Zandman-Goddard, G. & Shoenfeld, Y. Chapter 3 gender bias in Murine Lupus. *Handb. Syst. Autoimmune Dis.* **9**, 21–27 (2008).

23. Richard, M. L. & Gilkeson, G. Mouse models of lupus: what they tell us and what they don't. *Lupus Sci. Med.* **5**, e000199 (2018).

24. Yurkovetskiy, L. et al. Gender bias in autoimmunity is influenced by microbiota. *Immunity* **39**, 400–412 (2013).

25. Ngo, S. T., Steyn, F. J. & McCombe, P. A. Gender differences in autoimmune disease. *Front Neuroendocrinol.* **35**, 347–369 (2014).

26. Youness, A., Miquel, C. H. & Guery, J. C. Escape from X Chromosome inactivation and the female predominance in autoimmune diseases. *Int. J. Mol. Sci.* **22**, 1114 (2021).

27. Dai, R. & Ahmed, S. A. Sexual dimorphism of miRNA expression: a new perspective in understanding the sex bias of autoimmune diseases. *Ther. Clin. Risk Manag* **10**, 151–163 (2014).

28. Rubtsova, K., Marrack, P. & Rubtsov, A. V. Sexual dimorphism in autoimmunity. *J. Clin. Invest* **125**, 2187–2193 (2015).

29. Roubinian, J. R., Talal, N., Greenspan, J. S., Goodman, J. R. & Siiteri, P. K. Effect of castration and sex hormone treatment on survival, anti-nucleic acid antibodies, and glomerulonephritis in NZB/NZW F1 mice. *J. Exp. Med* **147**, 1568–1583 (1978).

30. Makino, S., Kunimoto, K., Muraoka, Y. & Katagiri, K. Effect of castration on the appearance of diabetes in NOD mouse. *Jikken Dobutsu* **30**, 137–140 (1981).

31. Chang, C., Yeh, S., Lee, S. O. & Chang, T. M. Androgen receptor (AR) pathophysiological roles in androgen-related diseases in skin, bone/muscle, metabolic syndrome and neuron/immune systems: lessons learned from mice lacking AR in specific cells. *Nucl. Recept Signal* **11**, e001 (2013).

32. Gilliver, S. C. Sex steroids as inflammatory regulators. *J. Steroid Biochem Mol. Biol.* **120**, 105–115 (2010).

33. Wilcoxen, S. C., Kirkman, E., Dowdell, K. C. & Stohlman, S. A. Gender-dependent IL-12 secretion by APC is regulated by IL-10. *J. Immunol.* **164**, 6237–6243 (2000).

34. Wen, L. et al. Innate immunity and intestinal microbiota in the development of Type 1 diabetes. *Nature* **455**, 1109–1113 (2008).

35. Markle, J. G. et al. Sex differences in the gut microbiome drive hormone-dependent regulation of autoimmunity. *Science* **339**, 1084–1088 (2013).

36. Davey, R. A. & Grossmann, M. Androgen receptor structure, function and biology: from bench to bedside. *Clin. Biochem Rev.* **37**, 3–15 (2016).

37. Heng, T. S., Painter, M. W. & Immunological Genome Project, C. The Immunological Genome Project: networks of gene expression in immune cells. *Nat. Immunol.* **9**, 1091–1094 (2008).

38. Consortium, E. P. et al. Expanded encyclopaedias of DNA elements in the human and mouse genomes. *Nature* **583**, 699–710 (2020).

39. Verdaguer, J. et al. Spontaneous autoimmune diabetes in monoclonal T cell nonobese diabetic mice. *J. Exp. Med* **186**, 1663–1676 (1997).

40. Wong, F. S. et al. Activation of insulin-reactive CD8 T-cells for development of autoimmune diabetes. *Diabetes* **58**, 1156–1164 (2009).

41. Varanasi, V., Avanesyan, L., Schumann, D. M. & Chervonsky, A. V. Cytotoxic mechanisms employed by mouse T cells to destroy pancreatic beta-cells. *Diabetes* **61**, 2862–2870 (2012).

42. Dunn, S. E. et al. Peroxisome proliferator-activated receptor (PPAR) alpha expression in T cells mediates gender differences in development of T cell-mediated autoimmunity. *J. Exp. Med* **204**, 321–330 (2007).

43. Guan, X. et al. Androgen receptor activity in T cells limits checkpoint blockade efficacy. *Nature* **606**, 791–796 (2022).

44. Yee Mon, K. J. et al. Differential sensitivity to IL-12 drives sex-specific differences in the CD8+ T cell response to infection. *Immunohorizons* **3**, 121–132 (2019).

45. Zhang, Y. et al. Model-based analysis of ChIP-Seq (MACS). *Genome Biol.* **9**, R137 (2008).

46. Szklarczyk, D. et al. The STRING database in 2011: functional interaction networks of proteins, globally integrated and scored. *Nucleic Acids Res.* **39**, D561–D568 (2010).

47. Kwon, H. et al. Androgen conspires with the CD8(+) T cell exhaustion program and contributes to sex bias in cancer. *Sci. Immunol.* **7**, eabq2630 (2022).

48. Yang, C. et al. Androgen receptor-mediated CD8(+) T cell stemness programs drive sex differences in antitumor immunity. *Immunity* **55**, 1268–1283 e1269 (2022).

49. Stanford, S. M. & Bottini, N. PTPN22: the archetypal non-HLA autoimmunity gene. *Nat. Rev. Rheumatol.* **10**, 602–611 (2014).

50. Bottini, N. & Peterson, E. J. Tyrosine phosphatase PTPN22: multifunctional regulator of immune signaling, development, and disease. *Annu Rev. Immunol.* **32**, 83–119 (2014).

51. Bottini, N. et al. A functional variant of lymphoid tyrosine phosphatase is associated with type I diabetes. *Nat. Genet.* **36**, 337–338 (2004).

52. Kyogoku, C. et al. Genetic association of the R620W polymorphism of protein tyrosine phosphatase PTPN22 with human SLE. *Am. J. Hum. Genet.* **75**, 504–507 (2004).

53. Begovich, A. B. et al. A missense single-nucleotide polymorphism in a gene encoding a protein tyrosine phosphatase (PTPN22) is associated with rheumatoid arthritis. *Am. J. Hum. Genet* **75**, 330–337 (2004).

54. Velaga, M. R. et al. The codon 620 tryptophan allele of the lymphoid tyrosine phosphatase (LYP) gene is a major determinant of Graves' disease. *J. Clin. Endocrinol. Metab.* **89**, 5862–5865 (2004).

55. Morel, L. et al. Genetic reconstitution of systemic lupus erythematosus immunopathology with polycongenic murine strains. *Proc. Natl Acad. Sci. USA* **97**, 6670–6675 (2000).

56. Hasegawa, K. et al. PEST domain-enriched tyrosine phosphatase (PEP) regulation of effector/memory T cells. *Science* **303**, 685–689 (2004).

57. Nielsen, C., Barington, T., Husby, S. & Lillevang, S. T. Expression of human PTPN22 alleles. *Genes Immun.* **8**, 131–137 (2007).

58. Zheng, J., Ibrahim, S., Petersen, F. & Yu, X. Meta-analysis reveals an association of PTPN22 C1858T with autoimmune diseases, which depends on the localization of the affected tissue. *Genes Immun.* **13**, 641–652 (2012).

59. Conrad, N. et al. Incidence, prevalence, and co-occurrence of autoimmune disorders over time and by age, sex, and socio-economic status: a population-based cohort study of 22 million individuals in the UK. *Lancet* **401**, 1878–1890 (2023).

60. Dultz, G. et al. The protein tyrosine phosphatase non-receptor type 22 C1858T polymorphism is a joint susceptibility locus for immunthyroiditis and autoimmune diabetes. *Thyroid* **19**, 143–148 (2009).

61. Frommer, L. & Kahaly, G. J. Autoimmune Polyendocrinopathy. *J. Clin. Endocrinol. Metab.* **104**, 4769–4782 (2019).

62. Frommer, L. & Kahaly, G. J. Type 1 Diabetes and autoimmune thyroid disease-the genetic link. *Front Endocrinol.* **12**, 618213 (2021).

63. Viselli, S. M., Olsen, N. J., Shults, K., Steizer, G. & Kovacs, W. J. Immunochemical and flow cytometric analysis of androgen receptor expression in thymocytes. *Mol. Cell Endocrinol.* **109**, 19–26 (1995).

64. Siminovitch, K. A. PTPN22 and autoimmune disease. *Nat. Genet* **36**, 1248–1249 (2004).

65. Kissick, H. T. et al. Androgens alter T-cell immunity by inhibiting T-helper 1 differentiation. *Proc. Natl Acad. Sci. USA* **111**, 9887–9892 (2014).

66. Maine, C. J. et al. The effect of the autoimmunity-associated gene, PTPN22, on a BXSB-derived model of lupus. *Clin. Immunol.* **156**, 65–73 (2015).

67. Zheng, P. & Kissler, S. PTPN22 silencing in the NOD model indicates the type 1 diabetes-associated allele is not a loss-of-function variant. *Diabetes* **62**, 896–904 (2013).

68. Maine, C. J. et al. PTPN22 alters the development of regulatory T cells in the thymus. *J. Immunol.* **188**, 5267–5275 (2012).

69. Menard, L. et al. The PTPN22 allele encoding an R620W variant interferes with the removal of developing autoreactive B cells in humans. *J. Clin. Invest.* **121**, 3635–3644 (2011).

70. Schickel, J. N. et al. PTPN22 inhibition resets defective human central B cell tolerance. *Sci. Immunol.* **1**, aaf7153 (2016).

71. Dai, X. et al. A disease-associated PTPN22 variant promotes systemic autoimmunity in murine models. *J. Clin. Invest.* **123**, 2024–2036 (2013).

72. Maine, C. J., Marquardt, K., Cheung, J. & Sherman, L. A. PTPN22 controls the germinal center by influencing the numbers and activity of T follicular helper cells. *J. Immunol.* **192**, 1415–1424 (2014).

73. Riegman, P. H., Vlietstra, R. J., van der Korput, J. A., Brinkmann, A. O. & Trapman, J. The promoter of the prostate-specific antigen gene contains a functional androgen responsive element. *Mol. Endocrinol.* **5**, 1921–1930 (1991).

74. Mitchell, S. H., Murtha, P. E., Zhang, S., Zhu, W. & Young, C. Y. An androgen response element mediates LNCaP cell dependent androgen induction of the hK2 gene. *Mol. Cell Endocrinol.* **168**, 89–99 (2000).

75. Nelson, C. C. et al. Determinants of DNA sequence specificity of the androgen, progesterone, and glucocorticoid receptors: evidence for differential steroid receptor response elements. *Mol. Endocrinol.* **13**, 2090–2107 (1999).

76. Wang, Q. et al. A hierarchical network of transcription factors governs androgen receptor-dependent prostate cancer growth. *Mol. Cell* **27**, 380–392 (2007).

77. Hay, C. W., Hunter, I., MacKenzie, A. & McEwan, I. J. An Sp1 modulated regulatory region unique to higher primates regulates human androgen receptor promoter activity in prostate cancer cells. *PLoS One* **10**, e0139990 (2015).

78. Wilson, S., Qi, J. & Filipp, F. V. Refinement of the androgen response element based on ChIP-Seq in androgen-insensitive and androgen-responsive prostate cancer cell lines. *Sci. Rep.* **6**, 32611 (2016).

79. Hay, C. W. et al. Negative regulation of the androgen receptor gene through a primate-specific androgen response element present in the 5' UTR. *Horm. Cancer* **5**, 299–311 (2014).

80. Zhu, M. L. et al. Sex bias in CNS autoimmune disease mediated by androgen control of autoimmune regulator. *Nat. Commun.* **7**, 11350 (2016).

81. Malchow, S. et al. Aire enforces immune tolerance by directing autoreactive T cells into the regulatory T cell lineage. *Immunity* **44**, 1102–1113 (2016).

82. Lin, X. et al. CRISPR-Cas9-mediated modification of the NOD mouse genome with Ptpn22R619W mutation increases autoimmune diabetes. *Diabetes* **65**, 2134–2138 (2016).

83. Cubas, R. et al. Autoimmunity linked protein phosphatase PTPN22 as a target for cancer immunotherapy. *J Immunother Cancer* **8**, e001439 (2020).

84. Ho, W. J. et al. Systemic inhibition of PTPN22 augments anticancer immunity. *J. Clin. Invest.* **131**, e146950 (2021).

85. Alexander, J. J., Chaves, L., Chang, A. & Quigg, R. J. The C5a receptor has a key role in immune complex glomerulonephritis in complement factor H-deficient mice. *Kidney Int.* **82**, 961–968 (2012).

86. Passwell, J., Schreiner, G. F., Nonaka, M., Beuscher, H. U. & Colten, H. R. Local extrahepatic expression of complement genes C3, factor B, C2, and C4 is increased in murine lupus nephritis. *J. Clin. Invest.* **82**, 1676–1684 (1988).

87. Amemiya, H. M., Kundaje, A. & Boyle, A. P. The ENCODE blacklist: identification of problematic regions of the genome. *Sci. Rep.* **9**, 9354 (2019).

88. Huang, W., Loganantharaj, R., Schroeder, B., Fargo, D. & Li, L. PAVIS: a tool for peak annotation and visualization. *Bioinformatics* **29**, 3097–3099 (2013).

89. Gillespie, M. et al. The reactome pathway knowledgebase 2022. *Nucleic Acids Res.* **50**, D687–D692 (2022).

Acknowledgements

Author contributions

A.V.C. conceived the project and supervised the research. J.L. and L.A.Y. performed experiments. D.R. analyzed single-cell sequencing data. L.F. performed human genetic analysis. Z.S. assisted J.L. with SLE analysis. A.C. performed analysis of the kidney pathology. G.J.K. organized data collection for the human cohort and supervised the analysis. A.A.K. contributed to the conceptualization of the project and supervised computational analysis. J.L., G.J.K., A.A.K. and A.V.C. contributed to the writing of the manuscript.

Competing interests

The Authors declare the following competing interests: A.A.K. receives compensation from 23andMe, Inc. The remaining authors declare no competing interests.

Additional information